Available online at www.sciencedirect.com
ScienceDirect
European Journal of Mechanics B/Fluids 28 (2009) 37–60

Weighted-residual integral boundary-layer model of temporally excited falling liquid films

Alexander Oron *, O. Gottlieb, Elena Novbari

Department of Mechanical Engineering, Technion – Israel Institute of Technology, Haifa 32000, Israel

Received 12 June 2007; received in revised form 4 November 2007; accepted 10 November 2007

Available online 15 February 2008

Abstract

The first-order time-modulated weighted-residual integral boundary layer (TMBL) equations are derived and analyzed. The non-linear dynamics of thin liquid films falling on a vertical oscillating plane is investigated numerically using these equations. The set of TMBL equations admits a solution corresponding to a flat film and a temporally periodic volumetric flow rate. Using Floquet theory we investigate stability of this solution. In the region of instability of time-periodic flow, forcing of the traveling wave and non-stationary wave regimes arising in the unmodulated system, results in the emergence of quasiperiodic and apparently chaotic regimes, respectively. The wave regimes of the γ_1- and γ_2-types survive the forcing imparted by plane oscillation. The possibility of the emergence of flow reversal is also addressed. The existence of regions of asymptotical stability of the flat film with a temporally periodic flow rate provides the window for reduction or even suppression of the waviness of the film interface. Numerical investigation of the non-linear dynamics of the modulated film confirms the analytical results arising from Floquet theory.
© 2008 Elsevier Masson SAS. All rights reserved.

Keywords: Falling films; Nonlinear dynamics; Bifurcations; Temporal modulation

1. Introduction

Falling liquid films are often encountered in various technological applications, such as evaporators, condensers, heat exchangers, coating, and physical phenomena, such as gravity currents and lava flows. Most of the theoretical and experimental work was carried out for the case where the solid surface underneath the falling film is static. For a review on this topic the reader is referred to Alekseenko et al. [1] and Chang [2].

Investigation of the influence of substrate oscillation on the dynamics of a horizontal liquid layer overlying it began four decades ago with the linear stability analysis of Yih [3] who carried out longwave expansions to determine domains of instability. Later, Or [4] revisited the Yih's problem and demonstrated using Floquet theory, that the instability sets in first for a finite-wavelength regime in a wide range of parameters. Halpern and Frenkel [5] studied the non-linear stability of a horizontal bilayer system subjected to the Rayleigh–Taylor instability when the substrate on the top of the heavier fluid layer performs in-plane oscillations. The fluid dynamics of the interface separating the

* Corresponding author. Fax: +972 4 8295711.
E-mail address: meroron@tx.technion.ac.il (A. Oron).

0997-7546/$ – see front matter © 2008 Elsevier Masson SAS. All rights reserved.
doi:10.1016/j.euromechflu.2007.11.007

two layers was investigated in terms of a weakly non-linear evolution equation of the Kuramoto–Sivashinsky type derived there for both low-frequency and high-frequency limits. In certain parameter domains, the Rayleigh–Taylor instability was shown to saturate due to planar oscillations. Thiele et al. [6] recently studied the dynamics of a thin liquid film subjected to the Marangoni and Faraday instabilities, the latter being triggered by substrate vibration in the direction normal to the substrate. They also gave an overview of the previous work on the dynamics of liquid films subjected to substrate oscillation in the normal direction.

Several experimental and theoretical investigations of falling liquid films on a periodically tangentially-oscillating solid surface have appeared in literature in the last two decades. Stability of the time-dependent base flow of a liquid layer with a deformable interface was investigated by Bauer and von Kerczek [7]. They used Floquet theory and found that in the limit of small wavenumbers, i.e., in the long-wave limit, the growth rate of disturbances is given by summation of the natural growth rate in the non-oscillating case driven by gravity and that due to pure oscillation in the horizontal case. More important, they also showed that for a certain range of the oscillation frequency, a falling film is stabilized provided that the Reynolds number of the flow is sufficiently small. Lin et al. [8] also used linear stability theory to demonstrate that periodic in-plane oscillation of the wall may suppress surface waves in certain windows of the system parameter space. They found that there exists more than one stability wedge with respect to the frequency of oscillation.

Tihon et al. [9] studied experimentally the behavior of liquid films flowing on a periodically oscillating inclined plane. Their measurements for forced plate vibrations depict superharmonics and a finite amplitude time-periodic response. Furthermore, they obtained aperiodic low amplitude response for excitation with increasing frequencies. They also found that oscillations with small amplitude or frequency are responsible for resonant excitation of waves with large amplitudes. On the other hand, their experiments showed that an increase of the oscillation frequency with fixed oscillation amplitude can lead first to an increase and then to a decrease of the amplitude of the interfacial wave.

Drahos et al. [10] studied experimentally the stability of two-dimensional waves falling on a vertical oscillating plane. Their experiments were carried out with non-Newtonian films that revealed a self-excited periodic wave for the case of a fixed plate. The vertical plate was perturbed with several forcing frequencies resulting in periodic, quasiperiodic and chaotic responses, which were analyzed using phase space reconstruction. They found that the plate oscillations led to the intensification of the wavy flow in some regimes and saturation of the surface waves amplitude in others. They also showed that the properties of the wavy flow do not depend on the amplitude of oscillation when the latter exceeds a certain value.

The dynamics of two-dimensional thin liquid films falling down a vertical wall periodically oscillating in its own plane with given amplitude and frequency was investigated [11]. A non-linear long-wave evolution equation referred to there as the temporally modulated Benney equation (TMBE) was derived and validated with respect to solutions obtained by direct numerical simulations [12]. Both the Benney equation [13,14] (BE) and TMBE [11,15] were numerically solved to investigate the fully non-linear film dynamics in the unforced and forced cases, respectively. The solutions of the BE were found to be of three different types: (i) linearly stable solutions decaying to the uniform state, (ii) linearly unstable bounded states, and (iii) linearly unstable unbounded solutions. The domain of linearly unstable bounded states was found to contain periodic traveling waves (TW), as well as temporally aperiodic non-stationary waves (NSW). All these were mapped into concise stability diagrams. The stability diagram of the TMBE was found to remain unchanged with respect to the BE for the investigated range of excitation parameters. However, the fundamental dynamical structure of the TMBE was shown to be quasi-periodic tori complemented by irregular aperiodic behavior of several types of strange attractors for sufficiently large frequency and amplitude of plane oscillation. These aperiodic responses were observed for unforced asymmetric uni- and bimodal waves at selected frequencies of excitation. A significant decrease of the maximal amplitude, or the roughness factor of the interfacial wave on relatively thick films, was achieved [11] with an increase of either amplitude or frequency of plane oscillation, qualitatively similar to the experiments of Tihon et al. [9].

The stability and bifurcations of parametrically excited thin falling liquid films using low-order truncation of the two-dimensional spatiotemporal dynamics as described by the TMBE were investigated [15]. A fourth-order modal dynamical system was validated to yield the primary bifurcation structure of the fundamental falling film dynamics described by the Benney equation (BE) and accurately predicted the quasi-periodic structure of the temporally modulated Benney equation (TMBE). The stability of fundamental steady and periodic solutions was analytically and numerically investigated, so as to reveal the threshold for non-stationary and chaotic solutions corresponding to aperiodic modulated traveling waves. The reduced modal dynamical system enabled construction of a comprehensive

bifurcation structure, which was verified by numerical solution of the evolution equation [15]. This analysis revealed that the chaotic response to temporal modulation was indeed an outcome of harmonic excitation of a quasiperiodic wave regime that was previously conjectured [16,17].

To overcome some of the drawbacks associated with the BE for fluids with large surface tension (large Kapitza number) an alternative approach was introduced by Ruyer-Quil and Manneville [18,19] extending the boundary-layer theory developed by Shkadov [20]. The Shkadov theory was shown [22,21] to be successful in describing the dynamics of falling films on static vertical and inclined substrates for intermediate Reynolds numbers ($R < 300$). However, it failed to match the linear stability threshold of the system, as was derived by Benjamin [23] using Orr–Sommerfeld equations, by Yih [24] employing long-wave expansions, and which is strictly satisfied by the BE. The theory developed by Ruyer-Quil and Manneville [18,19] for both first- and second-order approximations of the Navier–Stokes equations can be classified as weighted-residual integral boundary layer (WRIBL) theory. It corrected the inability of the Shkadov model equations to match the linear stability threshold of the system and was found to yield bounded solutions for a larger range of Reynolds numbers than in the case of the BE. Recently, Scheid et al. [25] carried out investigation of traveling wave solutions of the first-order WRIBL equations with various boundary conditions and compared them to those of the BE. However, the time-dependent evolution of the falling films, as described by the first-order WRIBL equations with periodic boundary conditions, has not yet been investigated.

A numerical investigation of the non-linear dynamics of thin falling films in the context of the first-order WRIBL equations derived by Ruyer-Quil and Manneville [18] was carried out by Oron et al. [26,27]. These equations, augmented with periodic boundary conditions have been shown to admit solutions of various kinds, among which one finds traveling waves (TW) and several types of aperiodic non-stationary waves (NSW). Coexistence of stable traveling wave (TW) flows of various types as well as TW and NSW were found to be possible [26] and Novbari [27]. It was also found there that traveling waves of the γ_1-type bifurcate from the stability threshold of the system and slightly before the parameter range, where the second mode becomes linearly unstable, a coexistence between the traveling waves of γ_1- and γ_2-types arises. The domain where traveling waves of the γ_2-type then become dominant and that where the γ_2-type waves lose stability to a non-stationary flow regime then follow. When more unstable modes become involved in the film dynamics, an increase in complexity of the spatiotemporal film dynamics occurs [26,27].

It is the purpose of this paper to develop a mathematical model for thin falling films on a periodically in-plane oscillating planar vertical surface based on the first-order model approach [18]. The paper is organized as follows: Section 2 is devoted to the formulation of the governing equations and derivation of the evolution TMBL equations. Section 3 deals with stability analysis of the temporally modulated system using Floquet theory. Section 4 briefly describes the numerical method and analysis' techniques employed here to study the fully non-linear regime of the film evolution. In Section 5 we validate the first-order TMBL equations by comparison of their solutions with the TMBE equation. In Section 6 we discuss the results of the numerical analysis of the evolution equations describing the film dynamics falling on a vertical oscillating plane. Section 7 is devoted to the amplitude reduction of the waves. Section 8 presents the concluding remarks.

2. Derivation of the evolution equations

We consider a two-dimensional flow of an isothermal liquid film of average thickness d on a solid planar surface oscillating in its own plane with specified amplitude and frequency and tilted at an angle θ with respect to the horizontal in a gravity field g. The relevant properties of the liquid are density ρ, kinematic viscosity ν and surface tension σ. The coordinate x is directed downwards along the plane, while y is normal to the plane.

Following [18] we choose the viscous length $l_s = \nu^{\frac{2}{3}}(g\sin\theta)^{-\frac{1}{3}}$ for scaling the spatial variables, the viscous time $T_s = \nu^{\frac{1}{3}}(g\sin\theta)^{-\frac{2}{3}}$ and the viscous velocity $u_s = \nu^{\frac{1}{3}}(g\sin\theta)^{\frac{1}{3}}$ for scaling time and the fluid velocities, respectively. The dimensionless surface tension defines the standard Kapitza number

$$\kappa = \frac{\sigma}{\sigma_s} = \sigma/\left(\rho\nu^{4/3}(g\sin\theta)^{1/3}\right) \tag{1}$$

of the fluid.

We start with the two-dimensional incompressible dimensionless Navier–Stokes (NS) equations governing the fluid flow, augmented by temporally modulated boundary conditions at the wall, the continuity equation, the balance of stresses and the kinematic condition, see Appendix A, Eqs. (A.1)–(A.5).

We now seek the solution of Eqs. (A.1)–(A.5) as perturbation series in powers of a small parameter $\varepsilon = d/\lambda$ defined as the ratio of the mean film thickness d and the characteristic wavelength of interfacial disturbance λ:

$$\begin{cases} u = u^0 + \varepsilon u^1 + \mathcal{O}(\varepsilon^2), \\ v = \varepsilon v^1 + \mathcal{O}(\varepsilon^2), \\ p = p^0 + \varepsilon p^1 + \mathcal{O}(\varepsilon^2). \end{cases} \tag{2}$$

Furthermore, we rescale the independent variables as $\xi = \varepsilon x$ and $\tau = \varepsilon t$, leaving the vertical variables y and h unstretched, as the long-wave regime of the film flow on a planar substrate is considered hereafter.

At first order in ε including the terms at order zero, the procedure yields upon returning to the original non-dimensional variables x and t, a set of boundary-layer equations [20]

$$\begin{cases} u_t + uu_x + vu_y - u_{yy} = 1 - Bh_x + \kappa h_{xxx}, \\ u_x + v_y = 0, \end{cases} \tag{3}$$

where superscripts of the expansions (2) have been dropped and $B = \cot(\theta)$. Note that the presence of the term κh_{xxx} in the first-order in ε boundary-layer Eqs. (3) is ensured for large Kapitza numbers, $\kappa = \mathrm{O}(\varepsilon^{-2})$.

A solid substrate oscillates in its own plane with the oscillation amplitude A and frequency Ω, thus the appropriate boundary condition for the longitudinal velocity u is $u|_0 = \alpha\zeta\cos(\zeta t)$, where the dimensionless oscillation amplitude and frequency are

$$\alpha = A/l_s, \qquad \zeta = \Omega T_s, \tag{4}$$

respectively.

We now consider the problem consisting of Eqs. (3) and the boundary conditions

$$\begin{cases} u|_0 = \alpha\zeta\cos(\zeta t), \quad v|_0 = 0, \\ u_y|_h = 0, \\ h_t + q_x = 0, \end{cases} \tag{5}$$

where $h = h(x,t), q = q(x,t)$ are, respectively, the local film thickness and the leading-order approximation of the volumetric flow rate scaled with ν

$$q = \int_0^h u\,dy. \tag{6}$$

In this work we employ the weighted-residual integral boundary layer approach, derived for the case of a static solid substrate by Ruyer-Quil and Manneville [18]. Following this approach the longitudinal fluid velocity component u is expanded in the form

$$u = \sum_{j=0}^{n} a_j f_j(\bar{y}) + b(t) f_{-1}(\bar{y}), \tag{7}$$

where $a_j = a_j(x,t)$ are slowly varying functions of its variables, $\bar{y} = y/h(x,t)$ is a spatial coordinate normal to the wall normalized by the local film thickness $h(x,t)$; $b(t) = \alpha\zeta\cos(\zeta t)$; $f_j = \bar{y}^{j+1} - \frac{j+1}{j+2}\bar{y}^{j+2}$, $j \geqslant 0$ are polynomials in $(0,1)$ forming a complete basis above differentiable functions u satisfying the conditions $u|_0 = 0$ and $u_{\bar{y}}|_1 = 0$. The monomial $f_{-1} \equiv 1$ is included to satisfy the oscillating boundary condition $u|_0 = \alpha\zeta\cos(\zeta t)$.

Similar to Ref. [18] it is assumed that the expansion coefficients $a_j(t)$, $j > 0$ are small, $\mathrm{O}(\varepsilon)$. Thus, small departures from the base state that combines the Nusselt flow represented by the parabolic profile f_0, and a rigid-body oscillation of the film represented by the b-term, are formally considered here.

The main milestones of the derivation of the evolution equations are given in Appendix B. Differentiating the x-component of the boundary-layer Eqs. (3), it is readily shown that the coefficients $a_1, a_2, \ldots, a_n$ and their derivatives are order ε, expressing the normal fluid velocity component v from the continuity equation and substituting the expansion (7) into the x-component of Eq. (3), neglecting all slowly varying terms of order ε^2 and retaining the terms

of order ε, yields a polynomial whose coefficients are equated to zero, order by order. This procedure provides the expressions for $a_0, \ldots, a_4$, Eqs. (B.1)–(B.5). Computing the local flow rate, as defined in Eq. (6), via the functions $b, a_0, \ldots, a_4$, as shown in Eq. (B.6), and solving for q_t, we obtain a set of two first-order evolution equations referred hereafter as to time-modulated weighted-residual integral boundary layer equations (TMBL)

$$h_t + q_x = 0, \tag{8a}$$

$$q_t = \frac{5}{6}h - \frac{5}{2}\frac{q}{h^2} - \frac{17}{7}\frac{qq_x}{h} + \frac{9}{7}\frac{q^2 h_x}{h^2} - \frac{5}{6}Bhh_x + \frac{5}{6}\kappa hh_{xxx} + \alpha\zeta\cos(\zeta t)\left(\frac{3q_x}{7} + \frac{5}{2h} - \frac{qh_x}{7h}\right) - \alpha\zeta^2\left(\frac{h}{6}\sin(\zeta t) + \frac{\alpha h_x}{7}\cos^2(\zeta t)\right). \tag{8b}$$

As suggested by the anonymous referee, Eq. (8b) can be formally obtained by assuming the streamwise component of the velocity field in the form $u = [\frac{3q}{h} - 3b(t)]f_0(y/h) + b(t)$, and integrating the first of Eq. (3) multiplied by f_0 over $0 \leqslant y \leqslant h$. We note that this assumption follows directly from Eq. (B.6).

The set of Eqs. (8a) and (8b) is valid in the case if $\alpha = \mathrm{O}(1)$, $\zeta = \mathrm{O}(1)$. In the case of $\alpha = \mathrm{O}(\varepsilon)$, $\zeta = \mathrm{O}(1)$, only the second and fourth terms in the time-dependent part of Eq. (8b) remain, while the other three are in this limit of order $\mathrm{O}(\varepsilon^2)$ and vanish from Eq. (8b).

Eqs. (8) are analytically and numerically investigated for various oscillation amplitudes and oscillation frequencies with periodic boundary conditions for both h and q in the domain $0 \leqslant x \leqslant L$ and for various initial conditions, one of them, namely

$$h(x, t=0) \equiv h_0(x) = h_N + \delta\sin\left(\frac{2\pi x}{L}\right), \quad \delta \ll 1, \tag{9a}$$

$$q(x, t=0) \equiv q_0(x) = q_N, \tag{9b}$$

is referred to as a "standard" initial condition. The value of δ is typically varied between 0.05 and 0.1. A use of periodic boundary conditions for Eqs. (8) with $\alpha = 0$, corresponding to the case of a static plane, was discussed and justified by comparison with several experimental data in the unmodulated case [26].

In the case of a vertical plane, $B = 0$, considered in this paper, the film thickness h_N and the volumetric flow rate q_N of the base Nusselt flow of the unmodulated case, are related to the Reynolds number $R = (gd^3)/(2\nu^2)$ based on the maximal value of the film velocity via

$$h_N = (2R)^{1/3}, \qquad q_N = \frac{1}{3}h_N^3, \tag{10}$$

respectively.

In order to compare the results of our investigation with other work available in the literature, it is important to relate between various values used elsewhere. Oron and Gottlieb [11] employed in their investigations of the first-order Benney equation the parameters R, the rescaled Weber number $\tilde{S} = 2\sigma/(3\rho g d^2)$ and the small order parameter ε defined as the ratio between the mean film thickness and the characteristic wavelength of the interfacial disturbance. We note that Salamon et al. [12] used the value of the Weber number, $W = \frac{3}{2}\tilde{S}$, whereas Scheid et al. [25] used the value of the Reynolds number based on the average film velocity, $Re = \frac{2}{3}R$, and the value of the fundamental wavenumber k corresponding to the size of the periodic domain of L. In addition to the relationships given in Eq. (10), these values are related by

$$L = \frac{2\pi}{k}, \quad \varepsilon = \frac{kh_N}{2\pi}, \quad \kappa = Wh_N^2. \tag{11}$$

3. Stability analysis of the modulated system

Non-dimensionalization of the problem variables with the scales used here, see Section 2, leads to the conclusion that the undisturbed state of the film of thickness d corresponds to $h = h_N \equiv (2R)^{1/3}$. Linear stability analysis of the state related to $h = h_N$ is carried out in this section. In what follows, only the case of a vertical plane $B = 0$ is considered.

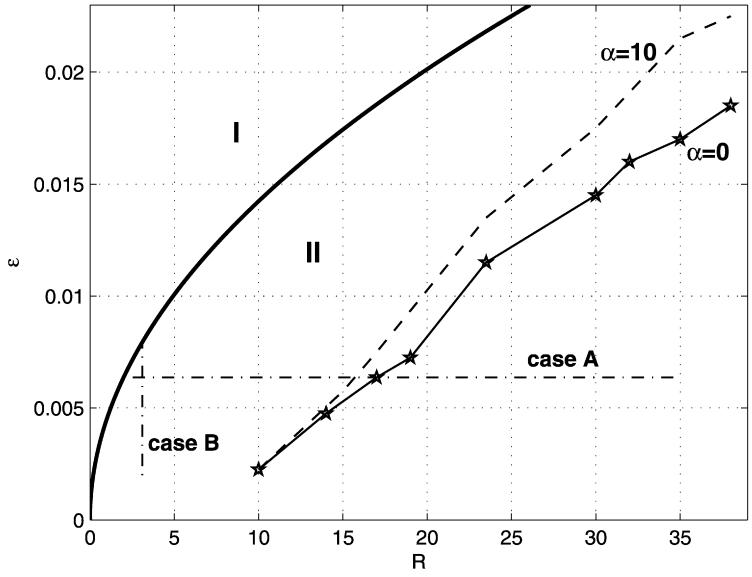

Fig. 1. Stability diagram for the unforced system with $W = 1000$. The bold solid curve represents the Hopf stability threshold. Region I is the domain of linear stability of the state $h = h_N$, while region II, below the curve is the instability domain. Horizontal and vertical dot-dashed lines show two cases, case A with $\varepsilon = 0.04/2\pi$ and case B with $R = 3.1$, where our numerical investigation has been carried out. The curve marked with asterisks represents the border line below which the value of $Q = q/q_N$ becomes negative for the unforced system, $\alpha = 0$. A reverse-flow border line for a modulated flow with the oscillation amplitude $\alpha = 10$ is marked by the dashed line.

We note some features of the stability analysis carried out for the unforced system [25,26] relevant for the analysis of the forced system. The solution $h = h_N$, $q = q_N$ of the WRIBL equations for the *unforced* system in the domain $[0, L]$ was found to be linearly stable [25–27] when $R < \frac{5}{4}(k^2\kappa + B)$. The conditions at the stability threshold are found to be $R = \frac{5}{4}B$ and $c = h_N^2$, where c is the critical frequency. These coincide with the corresponding results obtained by Benjamin [23] based on the Orr–Sommerfeld equations for the unforced system.

Fig. 1 displays the stability diagram of the state $h = h_N$ of the unmodulated system for $W = 1000$. The solid curve represents the Hopf stability threshold, $\varepsilon = (\sqrt{R/5W})/\pi$, of the unmodulated falling film and divides the $\varepsilon - R$ plane into two stability regions, one of which (I), located above this curve is the domain of linear stability of the state $h = h_N$, while (II), below the curve is that of its instability, both for the unmodulated film. Both, horizontal and vertical dot-dashed lines show the ranges, where our numerical investigation has been carried out in cases A ($\varepsilon = 0.04/2\pi$) and B ($R = 3.1$), respectively. It is worthwhile to note that the Hopf stability threshold is $R = 2$ in case A and $\varepsilon \approx 0.0079$ in case B. The curve marked with asterisks represents the border line below which the value of $Q = q/q_N$ becomes negative for the unforced system, while the dashed line displays the same phenomenon for the excited system when the normalized oscillation amplitude is $\alpha = 10$, both obtained numerically. Solutions with locally negative values of Q, will be shown to represent regimes with small spatial subdomains with recirculating flow. Such solutions were investigated for unmodulated flows in Refs. [26,27] and will be further discussed below in Section 6.3.

We note that $h = h_N$, $q = q_N$ is *not* a solution for Eqs. (8) for a forced system, $\alpha \neq 0$. Therefore, let us first establish a base state for the forced system whose stability will be investigated next.

Consider spatially uniform solutions for Eqs. (8) in the form

$$h = h_N, \qquad q = \bar{q}(t). \tag{12}$$

It then follows from Eq. (8b) that

$$\bar{q}(t) = const \cdot \exp(-\gamma t) + q_N + q_p(t), \tag{13a}$$

where

$$\gamma = \frac{5}{2h_N^2} \tag{13b}$$

and

$$q_p(t) = \frac{\alpha\zeta[(15\gamma + h_N^2\zeta^2)\cos(\zeta t) + (15 - \gamma h_N^2)\zeta \sin(\zeta t)]}{6h_N(\gamma^2 + \zeta^2)}. \tag{13c}$$

We note that the first component of Eq. (13a) depends on the initial condition via the value of *const* and decays exponentially in time. The second component represents q_N that is the flow rate of the Nusselt solution corresponding to the fixed point in the linearly stable domain. The third component $q_p(t)$ is time-periodic with a period equal to that of plane oscillation $2\pi/\zeta$ when $\alpha \neq 0$. Therefore, in the long-time range the solution $\bar{q}(t)$ is time-periodic with the average q_N.

To study stability of the solution $h = h_N, q = q_N + q_p(t)$ in the long-time range for $\alpha \neq 0$, we apply Floquet theory [28]. Eqs. (8) are linearized around this solution, $h = h_N + h',\ q = q_N + q_p(t) + q', |h'| \ll h_N,\ |q'| \ll q_N$, and the disturbance field is represented in the form

$$h' = \exp(ikx)\varphi(t), \qquad q' = \exp(ikx)\chi(t), \tag{14}$$

where k is the wavenumber of the disturbance. Then, from Eq. (8a) we find that $\chi = \frac{i}{k}\dot{\varphi}$, where a "dot" denotes differentiation with respect to t. From Eq. (8b) we find that the growth function $\varphi = \varphi(t)$ is complex and satisfies the complex differential equation

$$\ddot{\varphi} + U(t)\dot{\varphi} + V(t)\varphi = 0, \tag{15a}$$

where

$$\begin{aligned} U(t) &= \gamma + \frac{17ik}{7h_N}\hat{q}_p(t) - \frac{3}{7}i\alpha\zeta k\cos(\zeta t), \\ V(t) &= \frac{5ik}{6} + \frac{5ik}{h_N^3}\hat{q}_p(t) - \frac{9k^2}{7h_N^2}\hat{q}_p^2(t) + \frac{5}{6}Bh_Nk^2 + \frac{5}{6}\kappa k^4 h_N \\ &\quad - \left[i\gamma\alpha k\zeta - \frac{1}{7h_N}k^2\alpha\zeta\hat{q}_p(t)\right]\cos(\zeta t) - \frac{1}{6}i\alpha k\zeta^2\sin(\zeta t) + \frac{1}{7}k^2\alpha^2\zeta^2\cos^2(\zeta t), \end{aligned} \tag{15b}$$

where $\hat{q}_p(t) = q_N + q_p(t)$ and both $U(t)$, $V(t)$ are ζ-periodic in time.

Eq. (15) is rewritten in the form of four real ordinary differential equations of first order and solved numerically using the fourth-order Runge–Kutta method in the one-period domain $0 \leqslant t \leqslant \frac{2\pi}{\zeta}$ with the initial conditions corresponding to the unit matrix of order 4×4. This enables us to compute the monodromy matrix $\mathbf{M}$ and its eigenvalues. It follows from Floquet theory [28] that if the spectral radius of $\mathbf{M}$, $\rho(\mathbf{M})$ is smaller than one, the base time-periodic solution $q = q_N + q_p(t)$ is asymptotically stable, while if $\rho(\mathbf{M}) > 1$, the latter is unstable.

We found that the stability properties of the base state equation (12) change depending on whether the considered parameter set of the film is located in stability region I or II delineated earlier in this section.

In our numerical investigations reported below we focus on two parametric cases [12,11,15,25], namely: case A in which R varies with fixed $W = 1000$, $\varepsilon = 0.04/2\pi$; and case B in which ε varies with fixed $W = 1000$, $R = 3.1$.

We first discuss the stability properties of the base state equation (12) in region I. Fig. 2 displays the stability diagrams in case A with $R = 1$ and $R = 1.8$ and case B with $\varepsilon = 0.009$. In both, the curve $\alpha = \alpha_F(\zeta)$ separating between the domain of stability of the base state which is adjacent to the axis $\alpha = 0$ for $\zeta > \zeta_0$, and the domain of its instability above the curves is shown. The marginal curve $\alpha = \alpha_F(\zeta)$ is computed by applying Floquet theory and searching for the locus where $\rho(\mathbf{M}) = 1$. The curve $\alpha = \alpha_F(\zeta)$ has a concave shape and increases asymptotically for some values of ζ. Thus, the base state, Eq. (12) is asymptotically stable for both large and small values of ζ for all α. As the value of R approaches its Hopf threshold value for the unmodulated system, the domain of asymptotic stability of the base state, Eq. (12) shrinks for small ζ and widens for large ζ, as seen in Fig. 2. Fig. 3 presents the stability diagrams for the base state given by Eq. (12) in stability region II for Case A, $R = 7$ and $R = 15$, and Case B, $\varepsilon = 0.006$ and 0.004, respectively. Both of the figures display in the α–ζ plane the stability thresholds $\alpha = \alpha_F(\zeta)$ obtained by applying Floquet theory, as described in the previous paragraph. The domain above the curves represent the region of asymptotic stability of the base state (12), while below them, i.e., adjacent to the $\alpha = 0$ line, the latter is unstable. It follows from Fig. 3 that a larger distance from the linear stability threshold of the unmodulated system, namely a larger R in Case A and a smaller ε in Case B, leads to a higher oscillation frequency ζ needed for a fixed

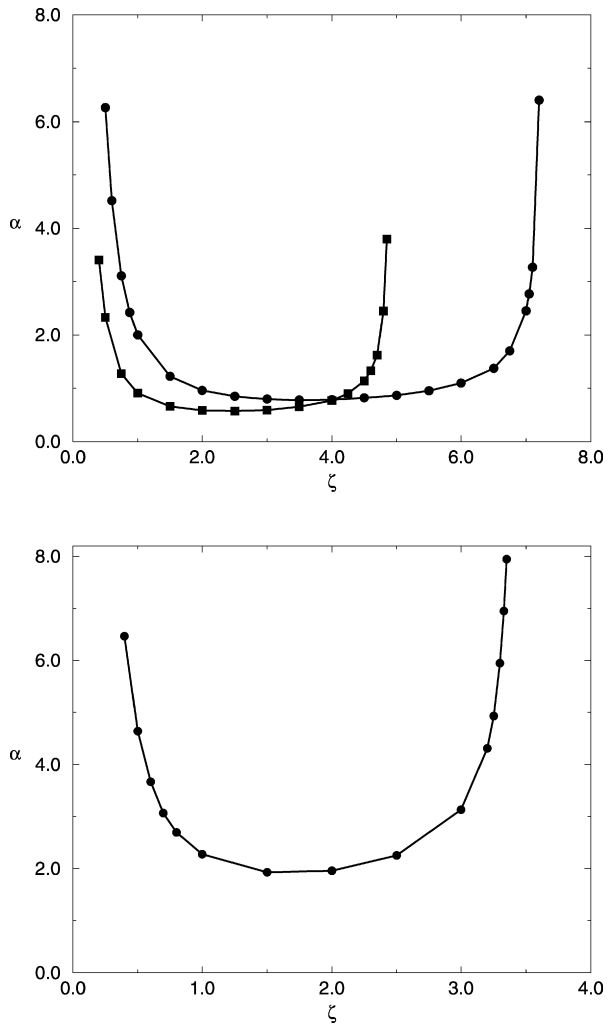

Fig. 2. The marginal curve $\alpha = \alpha_F(\zeta)$ for stability of the time-periodic base state, Eq. (12), corresponding to domain I. The domain of stability is located between the $\alpha = 0$ axis and the curve. The upper panel – case A, the curves marked by circles and squares correspond to $R = 1$ and $R = 1.8$, respectively; the lower panel – case B with $\varepsilon = 0.009$.

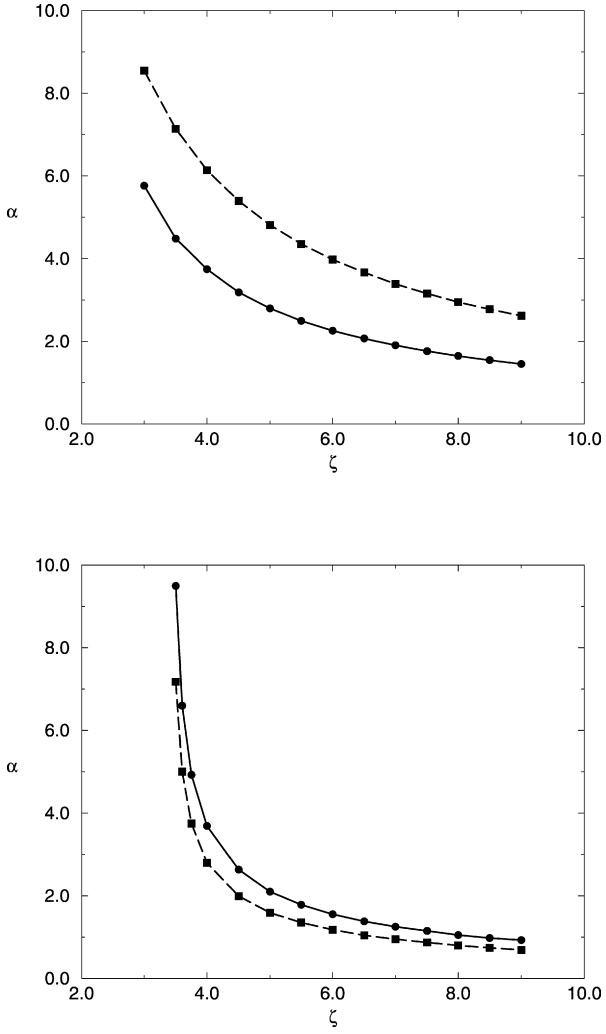

Fig. 3. The marginal curve $\alpha = \alpha_F(\zeta)$ for stability of the time-periodic base state, Eq. (12), corresponding to domain II. The domain of stability is located above the curve. The upper panel – case A with $R = 7$ (the lower curve) and $R = 15$ (the upper curve); the lower panel – case B, the upper and lower curves correspond to $\varepsilon = 0.004$ and 0.006, respectively.

α to stabilize the base state given by Eq. (12) and by this to suppress the waviness amplitude of the film. In both cases, along the stability curve the decrease of the oscillation amplitude $\alpha_F(\zeta)$ is accompanied with increase of the oscillation frequency ζ. We have also found that in both cases the stability curves do not extend into the region of $\zeta < \zeta_0$, for a certain ζ_0 and the oscillation amplitude α_F grows indefinitely when the frequency ζ approaches ζ_0 from the right. Therefore, the base state given by Eq. (12) is unstable for sufficiently small dimensionless frequencies ζ. It appears that the value of ζ_0 depends weakly on R in case A and on ε in case B. The consequences of this stability analysis will be discussed below in Section 7.

4. Numerical technique and analyses methodology

The numerical technique used here to solve Eqs. (8) is based on the Newton–Kantorovich method [29,11]. The method employed there is now extended to handle a set of coupled equations, similarly to Refs. [26,27].

Eqs. (8) are written in the form

$$\mathbf{y}_t = \mathbf{F}(\mathbf{y}, t), \tag{16}$$

where

$$\mathbf{y} = \begin{pmatrix} h(x,t) \\ q(x,t) \end{pmatrix}, \tag{17}$$

and

$$\mathbf{F} = \begin{pmatrix} \mathcal{H}(h,q;x,t) \\ \mathcal{Q}(h,q;x,t) \end{pmatrix} \tag{18}$$

with $\mathcal{H} = -q_x$ and $\mathcal{Q}$ given by the right-hand side of Eq. (8). To ensure the second-order accuracy of the solution in time we use the second-order, ($O(\Delta t^2)$), accurate Runge–Kutta method

$$\mathbf{y}^{(n+1)} = \mathbf{y}^{(n)} + \frac{1}{2}\Delta t\big[\mathbf{F}(\mathbf{y}^{(n+1)}, t_{n+1}) + \mathbf{F}(\mathbf{y}^{(n)}, t_n)\big], \tag{19}$$

where Δt is a time-marching step, the superscript (n) denotes the values of vector $\mathbf{y}$ at $t = t_n$. We employ Frechet differentials of the relevant operators to obtain from Eqs. (17), (18), a set of linear ordinary differential equations

$$\mathbf{J}\mathbf{v} \equiv \left[\mathbf{I} - \frac{1}{2}\Delta t\mathbf{F}_{\mathbf{y}}(\mathbf{y}^{(n)}, t_n)\right]\mathbf{v} = \Delta t\mathbf{F}(\mathbf{y}^{(n)}, t_n) \tag{20}$$

in terms of the vector $\mathbf{v}$ that constitutes the increment of the dependent variables between $t = t_n$ and $t = t_{n+1}$

$$\mathbf{v} \equiv \begin{pmatrix} \mathbf{v}_1 \\ \mathbf{v}_2 \end{pmatrix} = \begin{pmatrix} \mathbf{h}^{(n+1)} - \mathbf{h}^{(n)} \\ \mathbf{q}^{(n+1)} - \mathbf{q}^{(n)} \end{pmatrix}. \tag{21}$$

Here $\mathbf{v}_1, \mathbf{v}_2$ represent vectors that consist of values of the corresponding functions in the grid points, and $\mathbf{I}$ is a unit matrix.

The matrix $\mathbf{J}$ is a block $2N \times 2N$ matrix, where its upper $N \times 2N$ part arising from Eq. (8a) consists of the unit $N \times N$ matrix block on the left and a tridiagonal $N \times N$ matrix block with corner elements due to the periodic boundary conditions on the right. This structure of $\mathbf{J}$ allows to easily express the vector $\mathbf{v}_1$ via $\mathbf{v}_2$ at $t = t_n$ and by substituting it into the lower $N \times 2N$ block of Eq. (20) to finally arrive at

$$\left[\mathbf{I} - \frac{1}{2}\Delta t\mathbf{Q}_q(\mathbf{y}^{(n)}, t_n)\right]\mathbf{v}_2 + \frac{1}{4}(\Delta t^2)\mathbf{Q}_h(\mathbf{y}^{(n)}, t_n)\mathbf{v}_{2,x} = \Delta t\mathbf{Q}(\mathbf{y}^{(n)}, t_n) - \frac{1}{2}(\Delta t^2)\mathbf{Q}_h(\mathbf{y}^{(n)}, t_n)\mathbf{q}_x, \tag{22}$$

where $\mathbf{Q}_q, \mathbf{Q}_h$ are, respectively, Frechet-differential operators of $\mathcal{Q}$ with respect to q, h evaluated at $\mathbf{h} = \mathbf{h}^{(n)}, \mathbf{q} = \mathbf{q}^{(n)}$.

Eq. (22) represents a set of N linear ordinary differential equations which, upon spatial discretization using a finite differencing scheme based on a spatially uniform grid of the size Δx and accurate to second order in Δx, is reduced to a set of linear algebraic equations with a pentadiagonal matrix and triangular corners arising from the periodic boundary conditions. The latter is solved using the modified Thomas algorithm. Evaluation of the Frechet derivatives and spatial discretization are both carried out in the conservative form using linear interpolation for half-nodes, so that in the process of computations the total mass of the film is conserved up to $O(10^{-12})\%$ of the initial mass.

Eqs. (8) are numerically solved here using the spatially uniform grid of 700–1000 points and a typical initial adaptive time step of order 10^{-3}. During the computation of the spatiotemporal evolution of the film, the time series of the values of h, q and h_t, q_t at $x = 0$ are collected in the time range following the transient period for post-processing. The values of the time derivative q_t is estimated using the backward difference of first order accuracy in Δt. However, the value of h_t is computed directly from Eq. (8a) which is accurate to $O(\Delta t^2)$. These time series are further used to compute the portrait of the film evolution in the phase plane $(dH - H)$ and Poincaré maps. Here $H = h/h_N$, $dH \equiv h_t/h_N = -q_x/h_N$. The Poincaré maps presented below are defined by stroboscopic sampling the solution with the input forcing period $2\pi/\zeta$, where ζ is the dimensionless forcing frequency. We also compute and make use of the power spectra of the steady state temporal evolution.

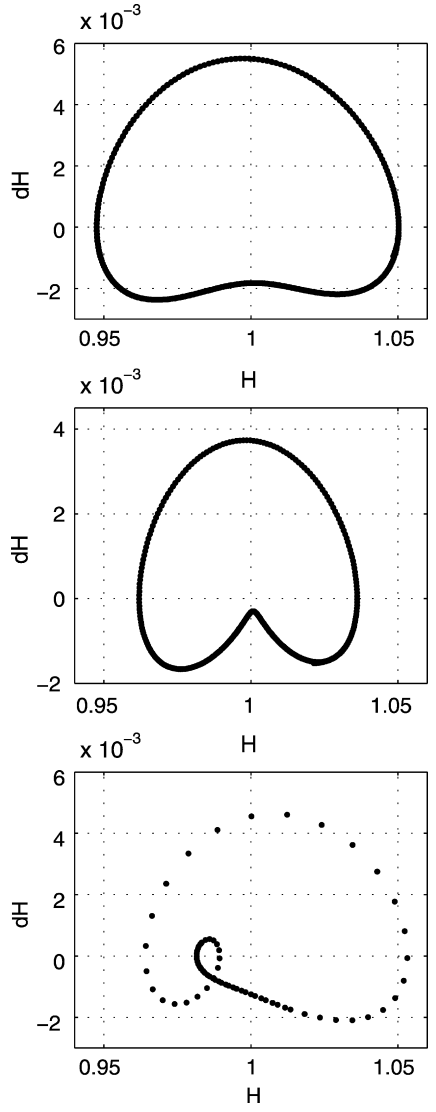

Fig. 4. Poincaré maps for $R = 3.1$, $W = 1000$, $\alpha = 1.837$. The panels from the top to the bottom correspond to $\varepsilon = 0.006$ and $\zeta = 0.07$; $\varepsilon = 0.004775$ and $\zeta = 0.055$; $\varepsilon = 0.003765$ and $\zeta = 0.043$, respectively. The maps show time intervals of: (a) $27\,000 < t < 55\,000$; (b) $30\,000 < t < 115\,000$; (c) $55\,000 < t < 70\,000$.

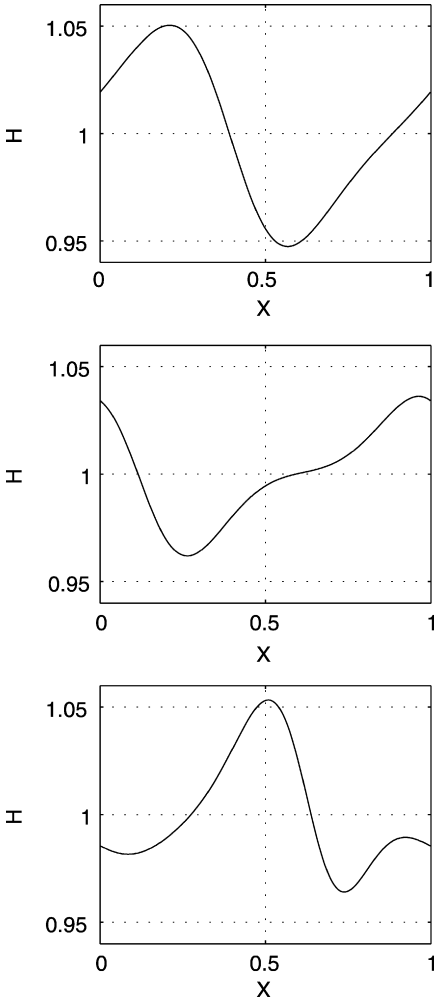

Fig. 5. The wave shapes for $R = 3.1$, $W = 1000$, $\alpha = 1.837$. The rows correspond to $\varepsilon = 0.006$ and $\zeta = 0.07$; $\varepsilon = 0.004775$ and $\zeta = 0.055$; $\varepsilon = 0.003765$ and $\zeta = 0.043$, respectively. Here $X = x/L$.

5. Comparison with TMBE

In this section we compare our numerical results for the temporally modulated system (TMBL) with those obtained by Oron and Gottlieb [11] for the TMBE equation.

Figs. 4 and 5 display the representative Poincaré maps and the wave shapes, respectively, for case B, i.e., $R = 3.1$, $W = 1000$. The panels from top to bottom correspond to $\varepsilon = 0.006$, 0.004775, 0.003765, respectively. The evolution of the time-modulated Benney equation (TMBE), [15] computed for the normalized oscillation amplitude $\tilde{\Gamma} = 1$ and frequency $\omega = 4\pi$ at $x = 0$ is presented in Figs. 5 and 6 in Ref. [15]. In order to compare with their results, we convert their parameters $\tilde{\Gamma}$ and ω to the non-dimensional oscillation amplitude α and frequency ζ used in Eqs. (8)

$$\zeta = \varepsilon\omega\frac{(2R)^{1/3}}{2}; \qquad \alpha = \tilde{\Gamma}(2R)^{1/3}. \tag{23}$$

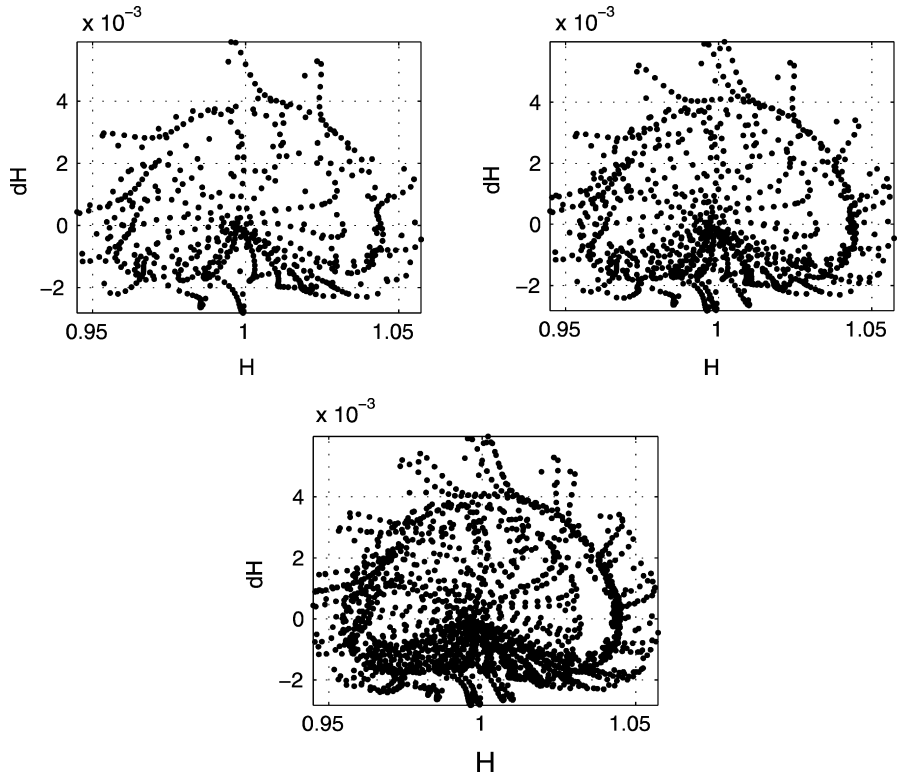

Fig. 6. The Poincaré maps in case B for $R = 3.1$, $W = 1000$, $\varepsilon = 0.003394$, $\alpha = 1.837$ and $\zeta = 0.039$, corresponding to the chaotic solution displayed in the middle row of Fig. 12. The maps include 600, 1000 and 2000 points per map, from the top to the bottom for $22\,500 \leqslant t \leqslant 116\,750$, for $22\,500 \leqslant t \leqslant 179\,580$, for $22\,500 \leqslant t \leqslant 336\,660$, respectively.

In Fig. 4 we depict quasiperiodic tori of TMBL for $\alpha = 1.84$ and $\zeta = 0.07, 0.055, 0.043$, respectively, while Fig. 5 shows that the spatial topological structure of the interfacial waves is not altered (TMBL versus TMBE), except for a slight change in the type of the solution. We use here the classification made by Chang [21] for the waves emerging in falling liquid films: (i) the γ_1-family whose representatives satisfy the condition $h_{\max} - h_N < h_N - h_{\min}$, i.e. depression or "hole" waves, and (ii) the γ_2-family whose representatives satisfy the condition $h_{\max} - h_N > h_N - h_{\min}$, i.e. elevation or "hump" waves. The TMBE yields γ_2-type solutions, whereas the TMBL equations show quasiperiodic solutions (QP) of the γ_1-family for the values of ε close to the Hopf threshold of the system ($\varepsilon = 0.006$, 0.004775, Fig. 4, Fig. 5 in the upper and middle panels) and γ_2-type QP solutions following the transition to the second mode ($\varepsilon = 0.003765$, Fig. 4, Fig. 5 in the lower panels). The maximal normalized value of the film thickness $H = h_{\max}/h_N$ is slightly lower than the value of $h_{\max}$ obtained by solving the TMBE by about 2%, but still shows a good agreement in terms of amplitudes.

However, we do not always obtain a good agreement between the solutions for TMBL and TMBE. Fig. 6 presents the Poincaré map of the chaotic solution for $\varepsilon = 0.003394$ with $\alpha = 1.837$ and $\zeta = 0.039$ for the TMBL equations. The upper map is obtained in the time interval $22\,500 \leqslant t \leqslant 116\,750$, while the others correspond to $22\,500 \leqslant t \leqslant 179\,580$ and $22\,500 \leqslant t \leqslant 336\,660$. The map for the TMBE corresponding to the top panel in Fig. 6 at the same value of ε and the corresponding non-dimensional forcing parameters is shown in Fig. 6(d3) [15] for $300 \leqslant t \leqslant 600$. Both of these maps contain 600 points each, but the strange attractors they depict are different in their internal structure and magnitude.

6. Numerical investigation

As noted above, we focus here on two cases considered [12,11,15,25], namely: case A in which $W = 1000$, $\varepsilon = 0.04/2\pi$; and case B in which $W = 1000$, $R = 3.1$. In both cases we employ periodic boundary conditions (referred to as closed flow conditions in Ref. [25]) in the domain $0 \leqslant x \leqslant L$, where $L = h_N \varepsilon^{-1}$. An alternative no-

tation [25] is $0 \leqslant x \leqslant 2\pi/k$, where k is the fundamental wavenumber, and the relationship between k and ε is given by:

$$k = \frac{2\pi\varepsilon}{(2R)^{1/3}}. \tag{24}$$

We investigate the dynamics of falling films on an oscillating vertical plane by numerically solving the TMBL equations (8) for values of parameters corresponding to case A and case B for various values of oscillation amplitude and frequency α and ζ, respectively. We recall that the Hopf stability threshold of the unmodulated system [26,27] is $\omega_{\text{Hopf}} = k(2R)^{2/3}$, where wavenumber k is defined by Eq. (24). We find from the solution of Eqs. (8) that in the unmodulated regime, the limit cycle frequency of the periodic traveling wave ω_{LC} is only slightly affected by the nonlinearities and is close to the value of the critical frequency obtained from the linear stability analysis of the unforced system

$$\omega_{\text{LC}} \sim \omega_{\text{Hopf}} = 2\pi\varepsilon(2R)^{1/3}. \tag{25}$$

We note that this value corresponds to the Hopf frequency 4π of the BE obtained by Oron and Gottlieb [11].

We solve Eqs. (8) with the oscillation frequency close to the natural frequency ω_{LC} obtained from the unforced case to investigate possible primary resonance and with frequencies of the excitation close to twice the natural frequency to investigate possible parametric resonance.

6.1. Case A

6.1.1. Bifurcation structure

We have found that the distinction between the subdomains $I - V$ found in Refs. [26,27] and reported below does not change in case A for different values of parameters α and ζ. The fundamental solution of the TMBL equations is found to be a quasiperiodic modulated propagating wave (QP) arising when the parametric excitation with $\alpha > \alpha_F(\zeta)$ in domain I and $\alpha < \alpha_F(\zeta)$ in domain II is applied to a periodic TW flow.

We obtain the following regions of stability corresponding to and modulated flows with $\alpha < \alpha_F(\zeta)$: (I) the region of the stability of $h = h_N$ for the unmodulated system, namely $R < 2$; (II) the domain where quasiperiodic flows of the γ_1-type emerge; (III) the region of coexisting QP solutions of both γ_1- and γ_2-types; (IV) the domain where quasiperiodic flows of the γ_2-type only emerge; (V) the domain where the solutions, QP for $16.5 < R \leqslant 31$ and $33 \leqslant R \leqslant 35$ and chaotic for $31 < R < 33$, exhibit the negative flow rates Q.

The regions I–V are intimately linked to regions I–V that were demarcated in Refs. [26,27] in case A for unmodulated films. As follows from our Floquet analysis in Section 3, the types of flow regimes obtained in regions I–V in

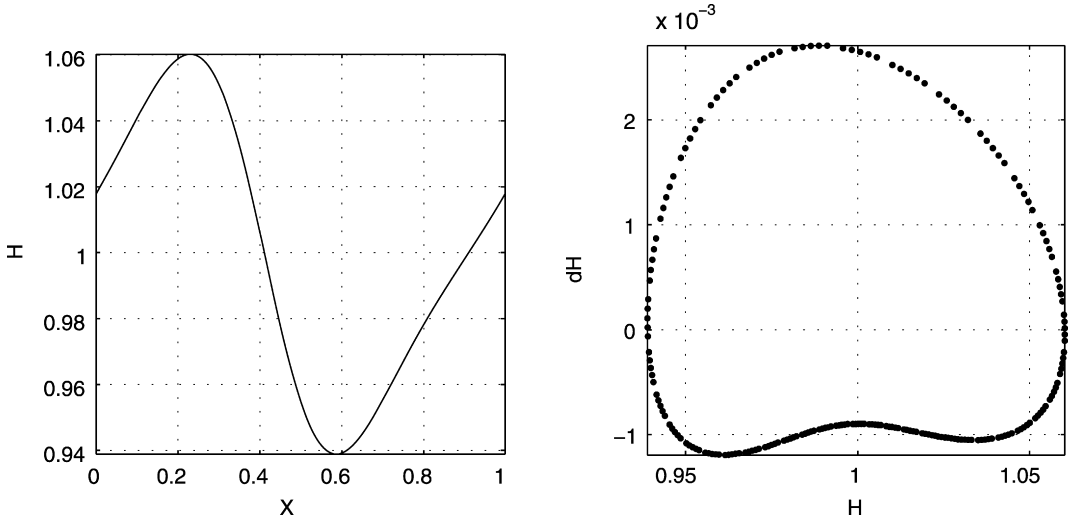

Fig. 7. The dynamics of the temporally modulated film in case A for $R = 1$ for $\alpha = 1.5$ and $\zeta = 2$. The wave shape of the film interface at $t = 64\,088$ and the Poincaré map for $63\,458 \leqslant t \leqslant 64\,088$ are presented.

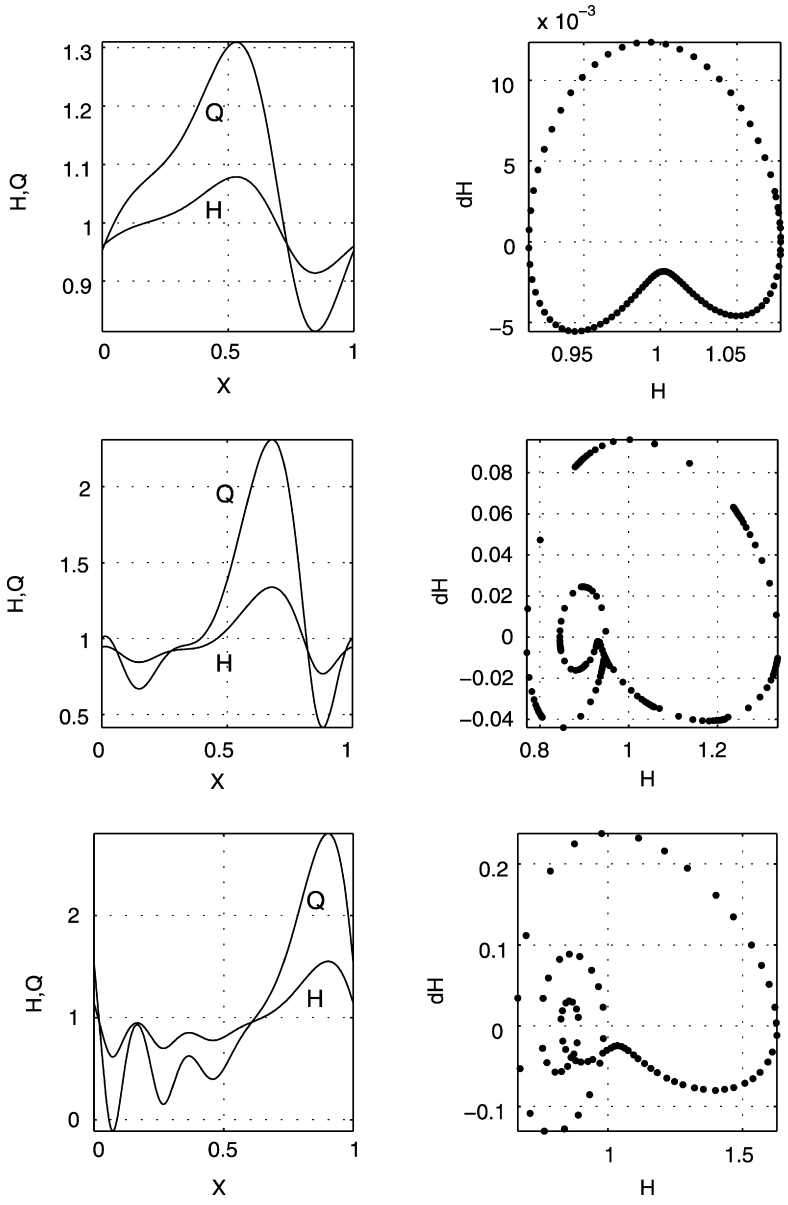

Fig. 8. The dynamics of the temporally modulated film in case A for various R and ζ, all for $\alpha = 2$. The first, second and third rows correspond to $R = 5$ and $\zeta = 0.086$, $R = 12$ and $\zeta = 0.115$, $R = 17$ and $\zeta = 0.1295$, respectively. The left column – the wave profiles of H and Q; the right column – the Poincaré maps of the corresponding solutions at $x = 0$ for $2000 < t < 8750$, $2000 < t < 6000$, $1000 < t < 4000$, respectively.

Refs. [26,27] for unmodulated flows, are preserved in the case of modulated flows with $\alpha > \alpha_F(\zeta)$. Also, the type of wave regimes, either γ_1 or γ_2, remains unaffected by plane oscillation.

6.1.2. Quasiperiodic solutions

When the film flow with $R = 1$ from within region I corresponding to a linearly stable unmodulated system is forced by $\alpha > \alpha_F(\zeta)$, the evolution of the standard initial condition leads to a quasiperiodic solution, as depicted in Fig. 7 where both the wave shape of the film interface and the Poincaré map of this flow are presented. Note that $X = x/L$ here and in the rest of the paper.

Fig. 8 presents the fundamental solutions of the TMBL equations, that are found to be quasiperiodic flows in region II, for $R = 5$, 12, 17, respectively, excited by oscillations with the limit cycle frequency of the corre-

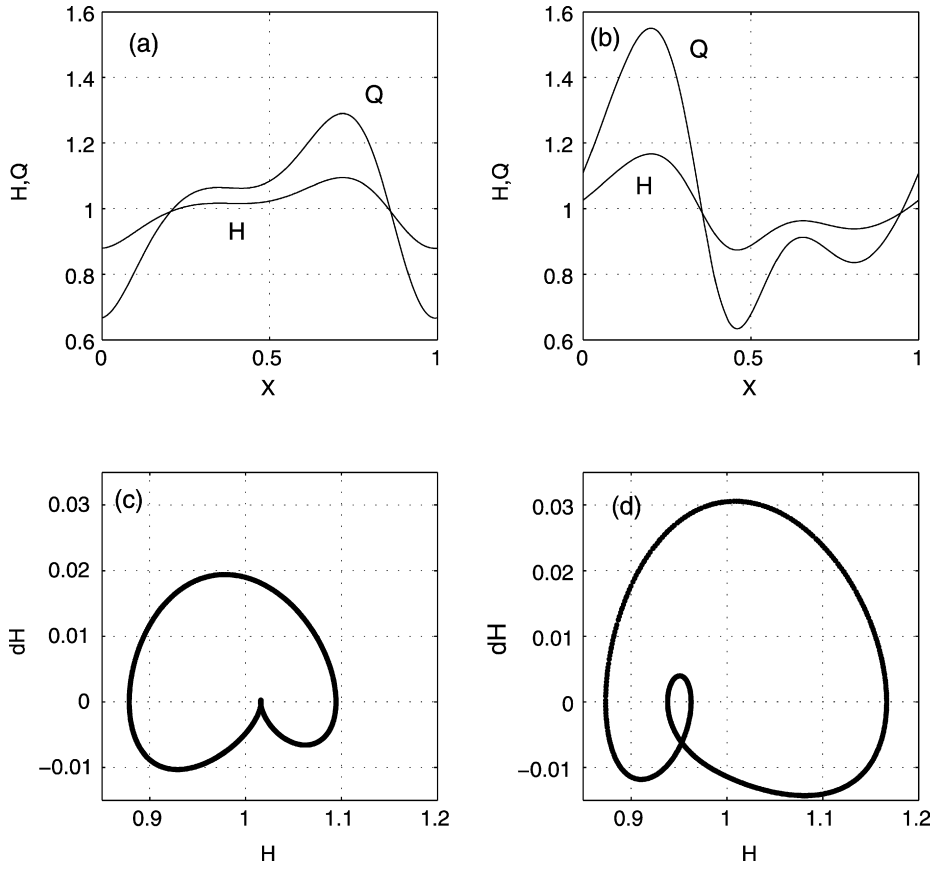

Fig. 9. Coexisting QP solutions in case A for $R = 7$. (a), (c): the γ_1-wave; (b), (d): the γ_2-wave; (a), (b) – the wave shapes $H(X)$, $Q(X)$ at $t = 17\,600$ and $t = 2500$, respectively; (c), (d) – the corresponding Poincaré maps at $12\,340 \leqslant t \leqslant 17\,600$ and $1750 \leqslant t \leqslant 2500$, respectively.

sponding unforced case $\zeta = 0.086$, 0.115, 0.1295, respectively. The oscillating amplitude $\alpha = 2 < \alpha_F(\zeta)$ was held fixed.

In the left column, Fig. 8 displays samples of both interfacial wave shapes $H(X)$ and spatial variation of the flow rate $Q(X)$, and in the right column, the Poincaré maps $dH(H)$. The Poincaré maps reveal the quasiperiodic character of film evolution. When the Reynolds number R increases, non-linearity of the solutions increases, as shown by the growing number of humps in the left column of Fig. 8. We notice topological similarity between the wave shapes and the identical γ_1-type of the solutions in both free and forced regimes and between the phase plane portraits and the Poincaré maps in both regimes [26,27].

6.1.3. Coexisting solutions

Numerical investigation of case A for the oscillating plane with $\alpha < \alpha_F(\zeta)$ reveals that subdomain (iii), $6.7 \leqslant R \leqslant 7.4$, is preserved as a region of coexistence of solutions that belong to γ_1- and γ_2-families. Fig. 9(a), (c) displays the wave shapes for both $H(X)$ and $Q(X)$, while Fig. 9(b), (d) shows the corresponding Poincaré maps $dH(H)$ for two, γ_1- and γ_2-type, quasiperiodic coexisting solutions in case A for $R = 7$, $\alpha = 2$, $\zeta = 0.093$ and $\zeta = 0.10$, respectively.

These QP solutions are an outcome of excitation of the unforced TW coexisting flows [26,27]. To obtain these solutions, we used the "standard" initial conditions for the γ_1-solution, and the corresponding solution for the BE as an initial condition for the γ_2-solution.

6.1.4. Chaotic solutions

When the parametric excitation with $\alpha < \alpha_F(\zeta)$ is applied to NSW flows, chaotic modulated propagating waves arise. Fig. 10 displays a chaotic-like solution obtained in case A for $R = 32$, $\alpha = 2$, $\zeta = 0.16$, presented by its sample wave shapes for both $H(X)$ and $Q(X)$ taken at a certain time t in Fig. 10-upper panel, by its Poincaré map $dH(H)$ in

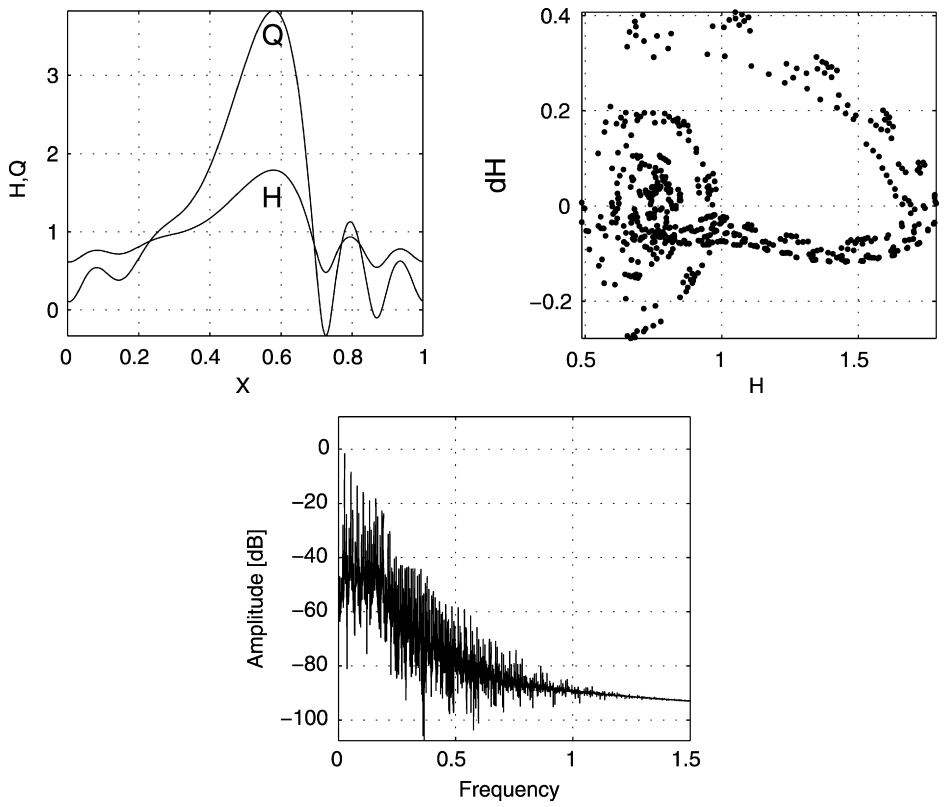

Fig. 10. Chaotic solution in case A for $R = 32$, $\alpha = 2$, $\zeta = 0.16$. the top left panel – the wave profile $H(X)$, $Q(X)$; the top right panel – Poincaré map for $1000 < t < 20\,000$, the bottom panel – the power spectrum of time series.

Fig. 10-middle panel, and the power spectrum of the time series in Fig. 10-lower panel. The power spectrum reveals an irregular spatiotemporal behavior characteristic of a chaotic strange attractor.

Excitation of the unforced film does not change the topological structure of the interfacial wave $H(X)$ and of the spatial variation obtained for $Q(X)$. However, we note that the flow rate $Q(X)$ is negative for $0.7 < X < 0.74$ at this time and displays a reverse flow in the corresponding subdomain of the periodic domain of the flow. This feature will be further discussed in Section 6.3.

6.2. Case B

6.2.1. Quasiperiodic solutions

In Section 5, we have showed the Poincaré maps (Fig. 4) and the wave shapes (Fig. 5) for the quasiperiodic solution of the TMBL equations for several values of ε from domain II and various values of the oscillation amplitude ζ. These solutions reveal that the interfacial waves remain topologically unchanged with respect to the unforced case and the Poincaré maps of the forced case resemble the phase plane portraits of the corresponding unmodulated case when $\alpha < \alpha_F(\zeta)$.

Fig. 11 presents the dynamics of the modulated film for $\varepsilon = 0.004775$ by eleven wave shapes $H(X)$ sampled each 10 time units during one forcing period $T = 2\pi/\zeta \approx 114.0$, where the forcing frequency is $\zeta = 0.055$. The wave propagates from the left to the right. One can notice that there is a slight change in shape of the wave with time, in particular in the domain around the inflection point between the trough and the crest of the wave.

6.2.2. Chaotic solutions

In Section 5 we presented the chaotic solution of the γ_2-type in case B, for $\varepsilon = 0.003394$, $\alpha = 1.837$ and $\zeta = 0.039$ by its Poincaré map, see Fig. 6, to compare our numerical investigations in case B with respect to the solutions of the

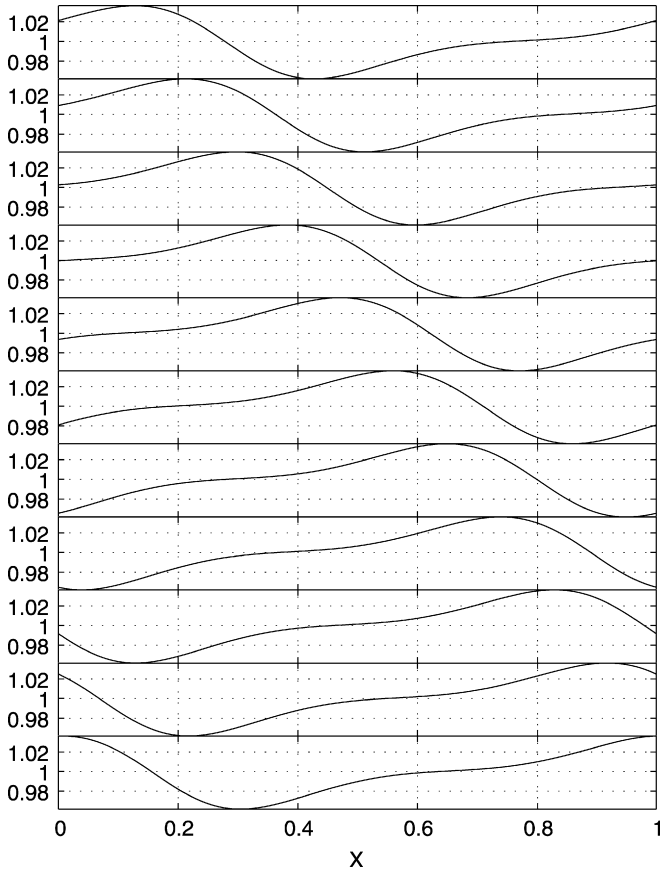

Fig. 11. The dynamics of the modulated film in case B: $R = 3.1$, $W = 1000$, $\varepsilon = 0.004775$, $\alpha = 1.84$, $\zeta = 0.055$. Eleven snapshots are shown in one forcing period equal to $T \approx 114$, the time difference between the snapshots is 10. The wave propagates from the left to the right.

TMBE equation [11]. This irregular regime is an outcome of excitation of the corresponding unforced γ_2-type NSW solution with $\alpha < \alpha_F(\zeta)$.

We studied the evolution of this solution for longer times. Fig. 6 shows three Poincaré maps consisting of 600, 1000 and 2000 points, respectively, from the top to the bottom for $22\,500 \leqslant t \leqslant 116\,750$, for $22\,500 \leqslant t \leqslant 179\,580$, for $22\,500 \leqslant t \leqslant 336\,660$. As follows from the comparison between these maps, the Poincaré points do not return each to other and the basic form of the cloud is preserved. This confirms the chaotic-like irregularity of the solution.

We have performed a numerical investigation for two additional values of ε close to $\varepsilon = 0.003394$, namely $\varepsilon = 0.0033$ and $\varepsilon = 0.0035$, and found that the solutions of the TMBL equations in these cases are also chaotic when $\alpha < \alpha_F(\zeta)$. The former is of the γ_1-type and the latter is of the γ_2-type, which correspond to the same type of a NSW solution in the unforced regime [26,27]. The right column of Fig. 12 presents the time series $H(t)$ at $x = 0$ for $\varepsilon = 0.0035$, $\zeta = 0.04$; $\varepsilon = 0.003394$, $\zeta = 0.039$ and $\varepsilon = 0.0033$, $\zeta = 0.038$, respectively, where all frequencies are near the primary resonance, all for $\alpha = 1.84$. Fig. 12 presents in its left column the Poincaré maps, consisting of 1000 points per map. Fig. 12 reveals in its left column additional types of strange attractors. While the Poincaré map of the solution for $\varepsilon = 0.0033$ (bottom-left) has a cloud form similar to $\varepsilon = 0.003394$, the map computed for $\varepsilon = 0.0035$ (top left) is different. The dynamics of $\varepsilon = 0.003394$, corresponding to the middle panel of Fig. 12, is shown in Fig. 13 by displaying several snapshots of the interfacial wave $H(X)$ sampled each 20 time units. Fig. 13 shows that the wave shapes are different each from the others and reveals an aperiodic in time structure of the chaotic solution.

6.2.3. Replicated waves

We have also found replicated waves of the γ_2-type consisting of two virtually identical humps. Fig. 14 presents such replicated wave obtained for $\varepsilon = 0.003$, the oscillation amplitude $\alpha = 1.84$ and the oscillation frequency near the

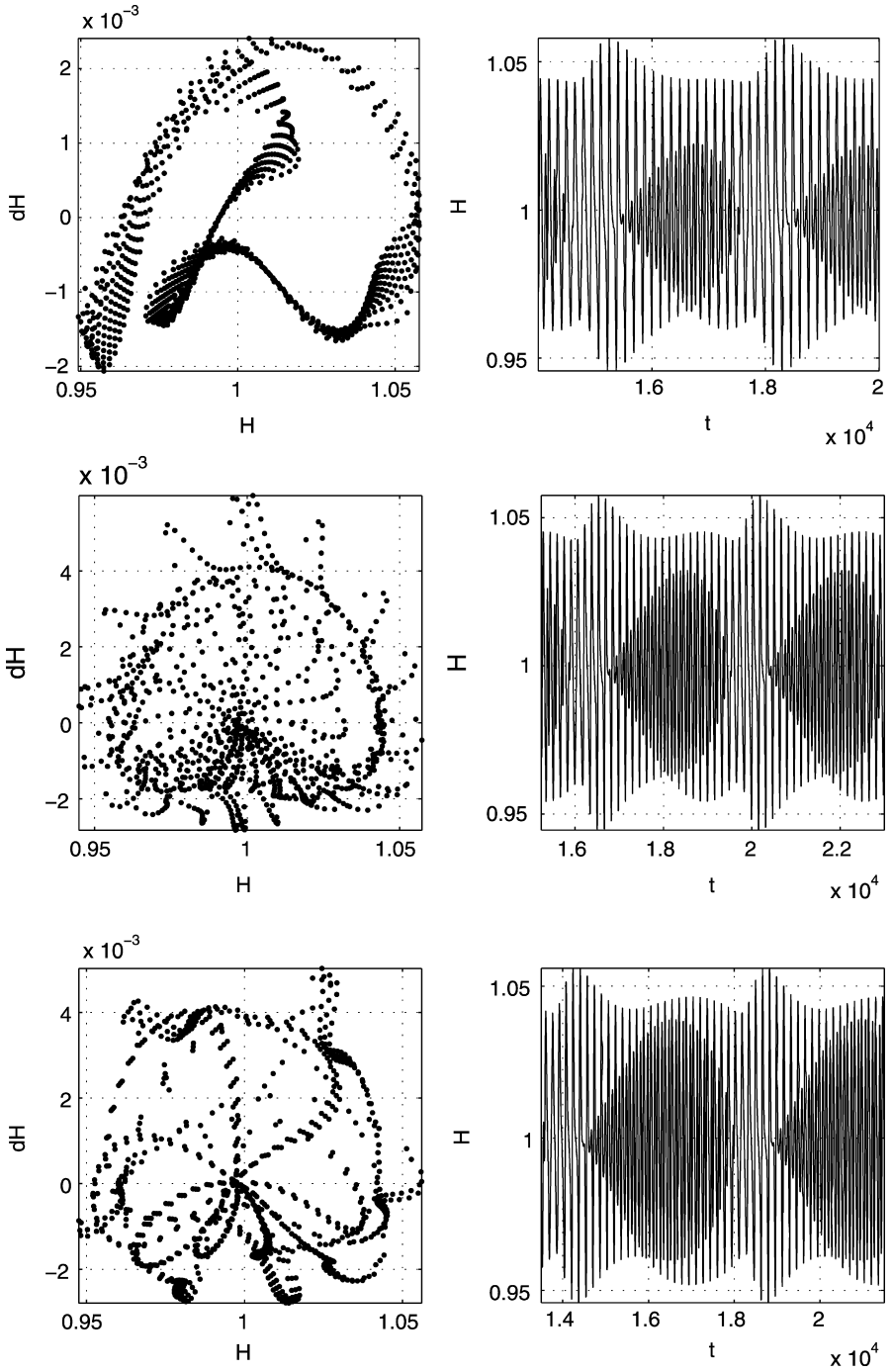

Fig. 12. The dynamics of the temporally modulated film in case B, $\alpha = 1.84$ for various ε and ζ. The first, second and third rows correspond to $\varepsilon = 0.0035$ and $\zeta = 0.04$, $\varepsilon = 0.003394$ and $\zeta = 0.039$, $\varepsilon = 0.0033$ and $\zeta = 0.038$, respectively. The left column – the Poincaré maps of the corresponding solutions at $x = 0$ for $20\,000 < t < 175\,525$, $76\,603 < t < 396\,598$, $21\,504 < t < 186\,451$, respectively. The right column – the time series of H at $x = 0$.

primary resonance $\zeta = 0.0346$ with $\alpha < \alpha_F(\zeta)$, by the interfacial shape $H(X)$ and the flow rate $Q(X)$ at $t = 20\,000$ in Fig. 14(a) and the corresponding Poincaré map in Fig. 14(b) for $15\,000 \leqslant t \leqslant 20\,000$.

The corresponding solution in the unforced regime for $\varepsilon = 0.003$ was found to be an aperiodic NSW flow from the γ_2-family [26,27]. Therefore, the outcome of its excitation would be expected to be a chaotic strange attractor.

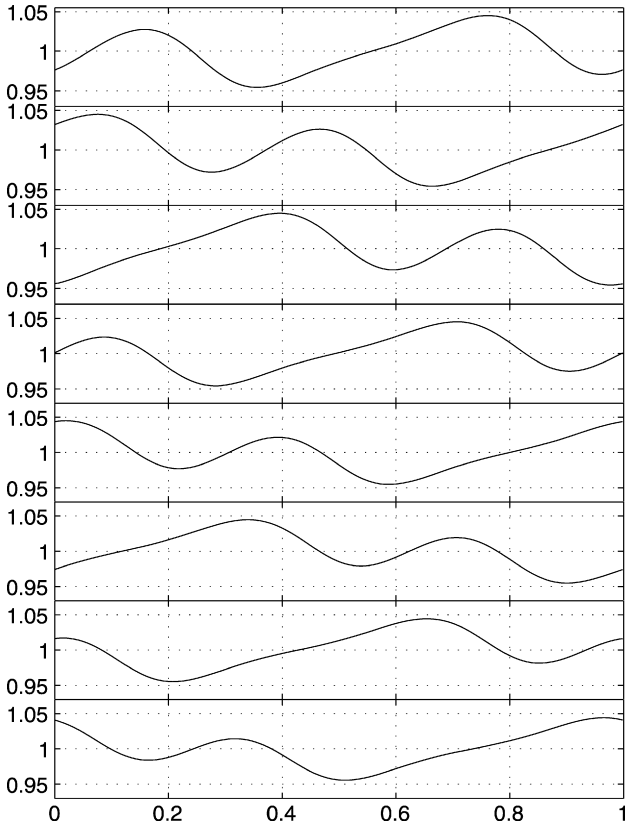

Fig. 13. The dynamics of the modulated film, as described by the TMBL equations, in case B for $R = 3.1$, $W = 1000$, $\varepsilon = 0.003394$, $\alpha = 1.84$, $\zeta = 0.039$, corresponding to the chaotic solution displayed in the middle panel of Fig. 12. Eight snapshots are shown with the time difference of 20 between the snapshots. The wave propagates from the left to the right.

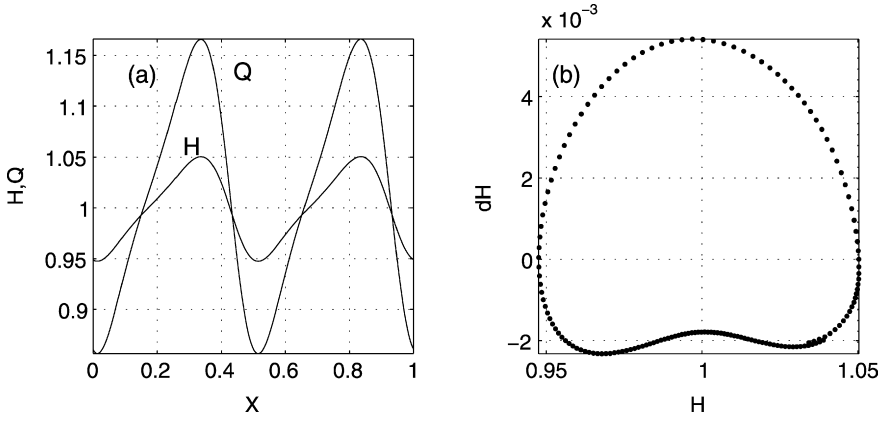

Fig. 14. A replicated wave that represents a quasiperiodic solution obtained in case B for $\varepsilon = 0.003$, $\alpha = 1.84$, $\zeta = 0.0346$. (a) The wave shapes $H(X)$ and $Q(X)$ at $t = 20\,000$; (b) The Poincaré map of this QP solution is presented for $15\,000 \leqslant t \leqslant 20\,000$.

However, Fig. 14 reveals a quasiperiodic character of film evolution. We note the difference in the wave amplitudes, namely, the maximal amplitude of the forced wave is much smaller than that of the unforced aperiodic wave [26,27]. Thus, we conjecture that there is a possible coexistence of this quasiperiodic solution and a chaotic attractor that may arise for a specific set of initial conditions.

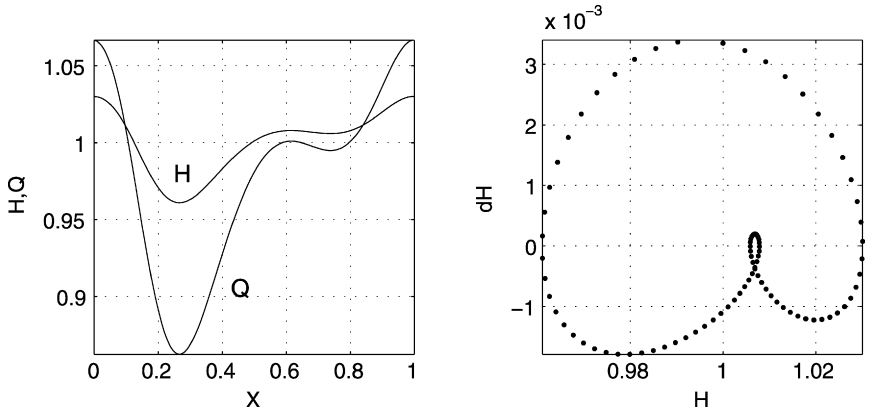

Fig. 15. A QP solution of the γ_1-type in case B for $\varepsilon = 0.00425$, $\alpha = 1.84$, $\zeta = 0.049$. The left panel shows the wave profiles $H(X)$, $Q(X)$ at $t = 40\,000$, while the right panel presents a Poincaré map for $30\,000 \leqslant t \leqslant 40\,000$. No solutions of the γ_2-type were found for this parameter set.

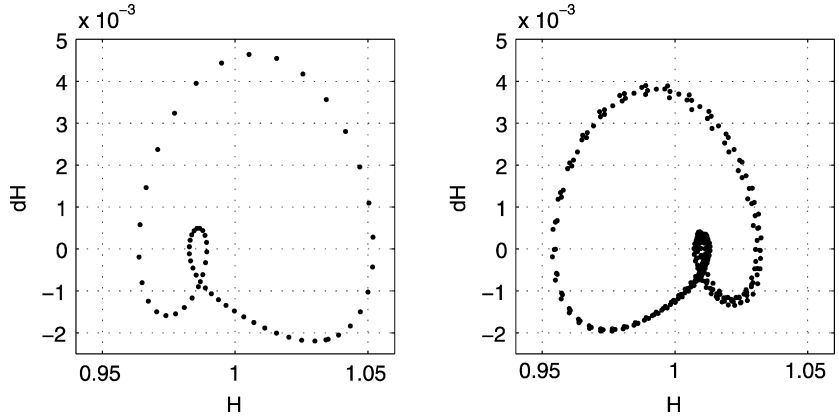

Fig. 16. Coexisting solutions in case B for $\varepsilon = 0.004$, $\alpha = 1.84$, $\zeta = 0.046$. The left panel corresponds to the γ_2-type QP solution, while the right panel shows the irregular solution of the γ_1-type; both represented by their Poincaré maps. A slight deviation of the Poincaré points from the curve does not disappear with a decrease of the time step of the numerical solution.

6.2.4. Coexisting solutions

Contrary to our prediction that the coexisting TW solutions of the γ_1- and γ_2-types obtained in case B, $\varepsilon = 0.00425$ in the unmodulated case [26,27], persist with excitation as quasiperiodic waves of the γ_1- and γ_2-families, we only find the γ_1-type QP solution for $\alpha = 1.84$ and $\zeta = 0.049$, despite multiple simulations for various kinds of the initial condition used in the unforced regime [26,27] to search for the γ_1- and γ_2-waves. This QP solution of the γ_1-type is presented in Fig. 15.

For $\varepsilon = 0.004$, we have obtained two coexisting solutions in the unforced regime [26,27]: the γ_2-type TW and NSW of the γ_1-type. As anticipated, when the parametric excitation with $\alpha = 1.84$ and $\zeta = 0.046$ ($\alpha < \alpha_F(\zeta)$), is applied to the γ_2-type TW solution, a quasiperiodic solution of the same γ_2-type arises. This solution is displayed in the left panel of Fig. 16 by its Poincaré map, whereas the right panel of Fig. 16 displays a more irregular coexisting solution of the γ_1-type.

6.3. Reverse flows of TMBL equations

Several studies [30–36] based on numerical solution of the Navier–Stokes equations suggest that in the case of an unmodulated falling films, a spontaneous return flow may emerge. In the case of a modulated system, the portions of the liquid adjacent to the oscillating wall are entrained during a half of the oscillation cycle in the flow upwards. However, the total flow rate in the cross-section may be still positive and return flow does not occur. This section is

devoted to the emergence of reverse flow that takes place where $Q(x) < 0$ at some location within the periodic domain and by continuity in its neighborhood.

In our previous study [26,27], we discussed the solutions of the WRIBL equations whose flow rate Q had a negative value. The loss of positivity for Q implies that the flow field displays a domain where a spontaneous return flow, against gravity, takes place. The negative sign of Q reveals that in the corresponding cross-sections of the film, the volumetric flow rate entrained in the return flow against gravity, is larger than that in the direction of gravity. We presented on the stability diagram for $W = 1000$ (Fig. 1 in Ref. [26]) the border line below which the value of Q becomes negative. In case A, the minimal value of $Q(X)$ vanishes at $R \approx 17$ and the WRIBL equations exhibit flow reversal in the unmodulated system for $R > 17$, where $Q(X)$ is negative for a certain range of X. In case B we have not encountered any evidence of flow reversal in the unmodulated case via the emergence of $Q < 0$.

In the present work, we investigate the flow reversal for Q for the TMBL equations. Fig. 1 displays the solid curve separating between the domain of positive Q located to the left of this line and that of negative Q located below this curve investigated for the WRIBL equations ($\alpha = 0, \zeta = 0$). We study the influence of the oscillation amplitude on the location of the curve along which $Q = 0$. The dot-dashed line reveals the loss of positivity of Q for the solutions of the TMBL equations for oscillation amplitude $\alpha = 10$ and oscillation frequency ζ_{LC} equal to that of the non-modulated film. We also find that for $\alpha = 18$, all the solutions below the stability threshold of the system ($n = 1$), including those of Case B and Case A, are regimes where flow reversal emerges.

7. Influence of oscillation on the wave amplitude

We have found that the amplitude of the interfacial waves can be reduced or even suppressed by harmonic temporal modulation of the substrate. To investigate the influence of the oscillation amplitude α and frequency ζ on the dynamics of the interfacial waves, we define first a suitable parameter associated with the reduction of the wave amplitude. Since the fundamental solution of the TMBL equations is quasiperiodic (QP), we cannot use the maximal value of the film thickness as such parameter. Instead, we introduce a roughness parameter [11] A,

$$A = \frac{(h_{\max} - h_{\min})^F}{(h_{\max} - h_{\min})^{UF}}, \tag{26}$$

where $h_{\max}$ and $h_{\min}$ are, respectively, the maximal and minimal film thickness, as determined in the saturated stage of evolution, and the superscripts ^{F} and ^{UF} correspond to the forced and to the natural, unforced, regimes, respectively.

Fig. 17 shows variation of A with the oscillation frequency ζ for three values of the oscillation amplitude $\alpha = 0.5; 1; 2$ in case B for $\varepsilon = 0.004775$ and for the range of the dimensionless oscillation frequency of $\zeta_{\mathrm{LC}} < \zeta < 220\zeta_{\mathrm{LC}}$, where in the case at hand $\zeta_{\mathrm{LC}} = 0.055$. The limiting value of $\zeta = 0$ corresponds to the case of a stationary solid plane, i.e., the unforced regime as described by the WRIBL equations [26,27], and in this case $A = 1$. When the oscillation frequency ζ increases ($\zeta_{\mathrm{LC}} < \zeta < 30\zeta_{\mathrm{LC}}$), the roughness factor also increases, i.e., in this range wall oscillation leads to the increase of the wave amplitude. When $\zeta > 30\zeta_{\mathrm{LC}}$, the value of A begins to decrease. We note that the parameter A returns to its starting value, $A = 1$, at approximately equal value of the oscillation frequency $\zeta \cong 60\zeta_{\mathrm{LC}}$, regardless of the oscillation amplitude α. For $\alpha = 2$ and $\zeta = 75\zeta_{\mathrm{LC}}$, we obtain about 20% decrease in the roughness factor A. If $\zeta = 85\zeta_{\mathrm{LC}}$, the reduction is 50%, while for $\zeta = 100\zeta_{\mathrm{LC}}$, the flow with an almost flat interface $h = h_N$ is obtained, i.e., $A \approx 0$.

Oron and Gottlieb [11] presented similar results found in the framework of the TMBE, namely, a small increase in A and following that a decrease of approximately 40% in the range of frequencies valid for the TMBE. Qualitatively similar results of the wave amplitude decrease with the oscillation frequency were presented in the experimental data obtained by Tihon et al. [9]. It is important to note that the Kapitza number of the fluid G85 used in the experimental studies of Tihon et al. [9] is about 12.0 which is not sufficiently large, as required in the derivation of Eqs. (8a) and (8b). This fact does not enable us to successfully validate our theoretical results with the experimental data [9].

The results related to suppression of the waviness of the film interface can be explained in terms of stability of the base state given by Eq. (12) according to the Floquet theory discussed in Section 3. In domain II, the stabilization was achieved by increasing either the normalized amplitude of plane oscillation α or its normalized frequency ζ. In

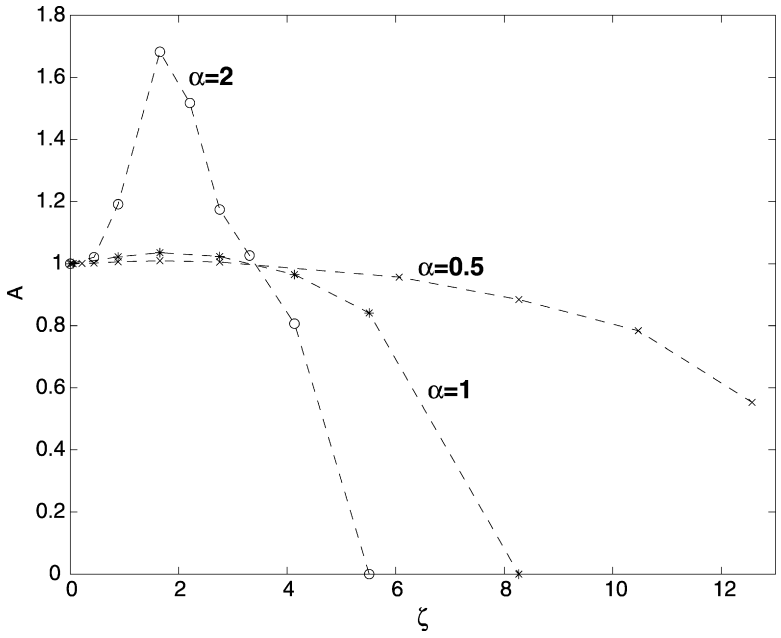

Fig. 17. The variation of the roughness factor A defined in Eq. (26) with the oscillation frequency ζ in case B for $\varepsilon = 0.004775$, $\alpha = 0.5$; 1; 2 and $0 < \zeta < 13$ corresponding to $0 < \zeta < 220\zeta_{\mathrm{LC}}$ with $\zeta_{\mathrm{LC}} = 0.055$. The dashed curves serve to guide the reader's eyes.

the stabilized regime, the long-time solution of the forced system exhibits flat interface $h = h_N$ and time-periodic dynamics of $q = q_p(t)$. The magnitude of the deviation of q from its mean value q_N is given by

$$q_m = \frac{\alpha\zeta\sqrt{225 + h_N^4\zeta^2}}{6h_N\sqrt{\gamma^2 + \zeta^2}} \tag{27}$$

and the numerical results based on Eqs. (8) perfectly fit it. The bounds of the stability domain based on Floquet analysis shown in Fig. 3 are also well reproduced by the numerical solution of Eqs. (8). Reduction of the wave amplitude described above also holds for apparently chaotic regimes. We note here that the same kind of stabilization and wave amplitude reduction has been also observed for forced water films. This is beyond the scope of this paper and will be discussed separately elsewhere.

Bauer and von Kerczek [7], and Lin et al. [8] demonstrated via Floquet theory applied directly to the linearized Navier–Stokes equations that windows of stabilization of the corresponding time-periodic solution of the Navier–Stokes equations emerge when plane oscillation is applied. These windows of stability expand when either the dimensionless amplitude or frequency of forcing increases. In our studies, however, we have not identified separate stabilization domains, but rather contiguous domains of stability. The reasons for this fact are yet unclear. One possibility may be the fact that the linear stability analysis of the time-periodic state was carried out in the framework of the original Navier–Stokes equations [7,8], while in our analysis the framework is the long-wave approximate TMBL equations. Another explanation may be the differences in the base states, Eq. (12) and the base solution presented by Lin et al. [8]. Fig. 18 presents a comparison between these two base states which are both ζ-periodic in time and are shown in one period $0 \leqslant t \leqslant 2\pi/\zeta$. As follows from Fig. 18, apart from a slight phase shift between the solutions, there is a discrepancy between them which grows with α and reaches about 10% in the flow rate amplitude.

8. Conclusions

In this paper we have derived and analyzed the spatiotemporal dynamics of thin liquid films falling on an oscillating vertical plane via the time-modulated weighted-residual boundary-layer (TMBL) equations. This set of evolution

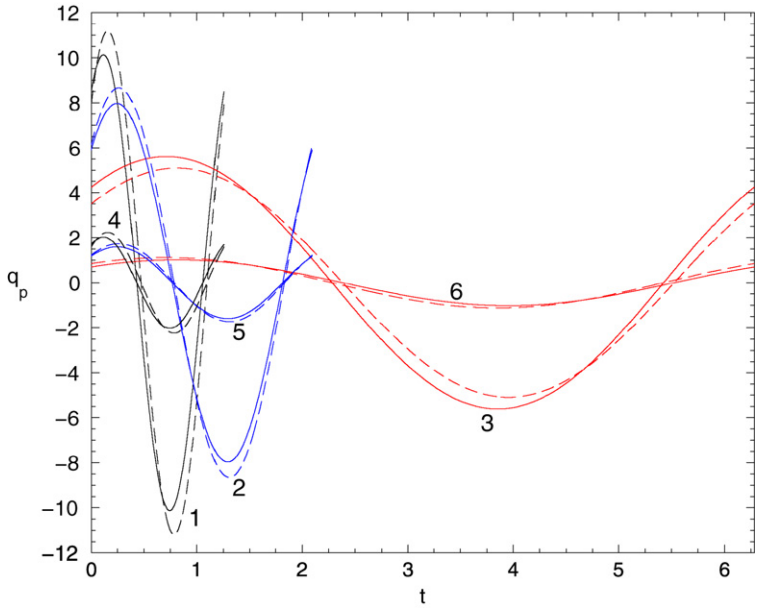

Fig. 18. A comparison between the base state (Eq. (12)) shown by solid curves and that derived by Lin et al. [8] shown by dashed curves both presented in one period time interval $0 \leqslant t \leqslant 2\pi/\zeta$. Curves 1–6 correspond, respectively, to pairs (α, ζ) given by (5, 1); (5, 3); (5, 5); (1, 1); (1, 3) and (1, 5).

equations represents an approximation to the Navier–Stokes equations with appropriate boundary conditions to the first order of the small aspect ratio parameter.

The set of TMBL equations admits a solution that corresponds to a flat film and temporally periodic volumetric flow rate. Using Floquet theory we have demonstrated that there exists a region in the plane spanned by the dimensionless oscillation amplitude and frequency, where this solution is asymptotically stable. In the domain of linear stability of the Nusselt flow of the non-modulated system, the region of asymptotical stability (AS) of the time-periodic state is for small forcing amplitudes, while in the domain of the instability of the Nusselt flow the region of AS of the temporally periodic flow is for sufficiently large forcing amplitudes depending on the oscillation frequency.

We have found that in the region of instability of the temporally periodic flow, forcing of the traveling wave and non-stationary wave regimes arising in the unmodulated system results in the emergence of quasiperiodic and apparently chaotic regimes, respectively. These regions correspond exactly to the TW and NSW solutions of the unmodulated system. Furthermore, the wave regimes of the γ_1- and γ_2-types survive forcing imparted by plane oscillation.

The possibility of the emergence of reverse flows has been also addressed in the paper. The border line delineating the appearance of reverse flow and its variation with respect to the forcing parameters have been determined. We have also found that an increase of the modulation amplitude leads to expansion of the domain of flow reversal, especially for larger values of the Reynolds number, where it extends even into the parameter domain with one linearly unstable mode. We have also revealed that for a sufficiently large oscillation amplitude, all flows display the feature of reversal. The results of our investigation show that the topological shape of the interfacial wave does not change as a result of plane oscillation whether flow reversal emerges or not.

Finally, the existence of the regions of asymptotical stability of the flat film with a temporally periodic flow rate provides the window for reduction or even suppression of the waviness of the film interface in both domains of linear stability and instability of the non-modulated falling films. Numerical investigation of the non-linear dynamics of the modulated film confirms the analytical results arising from the linear theory based on Floquet analysis. We have found that the domains of the wave amplitude suppression obtained from the numerical solution of the TMBL equations are roughly delineated by the borders of the stability regions derived from Floquet theory.

Acknowledgements

A.O. and O.G. were partially supported by the Technion President Fund and the Fund for Promotion of Research at the Technion. E.N. was partially supported by Dr. Jacob Isler Foundation. We also thank the anonymous referees for their useful remarks.

Appendix A. Dimensionless equations and boundary conditions

The dimensionless governing continuity and Navier–Stokes equations are

$$\begin{cases} u_x + v_y = 0, \\ u_t + uu_x + vv_y = -p_x + 1 + u_{xx} + u_{yy}, \\ v_t + uv_x + vv_y = -p_y - \cot\theta + v_{xx} + v_{yy}. \end{cases} \tag{A.1}$$

The corresponding boundary conditions at the wall ($y = 0$) are no-slip-no-penetration conditions:

$$u|_0 = \alpha\zeta \cos(\zeta t), \qquad v|_0 = 0. \tag{A.2}$$

At the free surface $y = h(x,t)$, the boundary conditions are the balance of normal and tangential stresses calculated by projecting the stress vector onto the normal and the tangential directions to the film interface, respectively,

$$\frac{\kappa h_{xx}}{[1+(h_x)^2]^{3/2}} + \frac{2}{1+(h_x)^2}\big[h_x(u_y|_h + v_x|_h) - (h_x)^2 u_x|_h - v_y|_h\big] + p|_h = 0, \tag{A.3}$$

$$2h_x(v_y|_h - u_x|_h) + \big[1-(h_x)^2\big](u_y|_h + v_x|_h) = 0, \tag{A.4}$$

and the kinematic condition is

$$h_t + u|_h\, h_x = v|_h. \tag{A.5}$$

Appendix B. Derivation of Eqs. (8)

This appendix contains the main milestones of the derivation of Eqs. (8).

Following essentially the derivation procedure proposed by Ruyer-Quil and Manneville [18] for the case of a static wall, we find the expressions for the coefficients $a_0, \ldots, a_4$ of the expansion (7) up to order ε

$$\begin{aligned} a_0 = {} & h^2 - \frac{1}{3}h^2\partial_t a_0 + \frac{1}{6}ha_0h_t - \frac{1}{10}h^2a_0\partial_x a_0 + \frac{1}{30}ha_0^2h_x - Bh^2h_x + \kappa h^2h_{xxx} \\ & + \alpha\zeta\cos(\zeta t)\left(\frac{h}{6}a_0h_x - \frac{h^2}{3}\partial_x a_0\right) + \alpha\zeta^2h^2\sin(\zeta t), \end{aligned} \tag{B.1}$$

$$a_1 = \frac{h}{12}a_0h_t + \frac{h}{60}a_0^2h_x - \frac{h^2}{6}\partial_t a_0 - \frac{h^2}{20}a_0\partial_x a_0 + \alpha\zeta\cos(\zeta t)\left(\frac{h}{12}a_0h_x - \frac{h^2}{6}\partial_x a_0\right), \tag{B.2}$$

$$a_2 = -\frac{h}{9}a_0h_t + \frac{h}{90}a_0^2h_x + \frac{h^2}{18}\partial_t a_0 - \frac{h^2}{30}a_0\partial_x a_0 - \alpha\zeta\cos(\zeta t)\left(\frac{h}{9}a_0h_x - \frac{h^2}{18}\partial_x a_0\right), \tag{B.3}$$

$$a_3 = -\frac{h}{30}a_0^2h_x + \frac{h^2}{60}a_0\partial_x a_0, \tag{B.4}$$

$$a_4 = \frac{h}{150}a_0^2h_x - \frac{h^2}{300}a_0\partial_x a_0. \tag{B.5}$$

The flow rate q is expressed as

$$\begin{aligned} q &= h\left(b + \sum_{j=0}^{4} a_j \int_0^1 f_j\, d\bar{y}\right) \\ &= \frac{1}{3}h\left(3\alpha\zeta\cos(\zeta t) + a_0 + \frac{1}{2}a_1 + \frac{3}{10}a_2 + \frac{1}{5}a_3 + \frac{1}{7}a_4\right), \end{aligned} \tag{B.6}$$

and the derivation of the evolution equation (8b) is concluded by differentiation of Eq. (B.6) with respect to time and taking into account slow variation of a_i, $i \geqslant 1$ with t, [27].

References

[1] S.V. Alekseenko, V.E. Nakoryakov, B.G. Pokusaev, Wave Flow of Liquid Films, Begell House, New York, 1994.
[2] H.C. Chang, E.A. Demekhin, Complex Wave Dynamics on Thin Films, Elsevier, Amsterdam, 2002.
[3] C.-S. Yih, Instability of unsteady flows or configurations. Part 1. Instability of a horizontal liquid layer on an oscillating plane, J. Fluid Mech. 31 (1968) 737.
[4] A.C. Or, Finite-wavelength instability in a horizontal liquid layer on an oscillating plane, J. Fluid Mech. 335 (1997) 213.
[5] D. Halpern, A.L. Frenkel, Saturated Rayleigh–Taylor instability of an oscillating Couette film flow, J. Fluid Mech. 446 (2001) 67.
[6] U. Thiele, J.M. Vega, E. Knobloch, Long-wave Marangoni instability with vibration, J. Fluid Mech. 546 (2005) 61.
[7] R.J. Bauer, C.H. von Kerczek, Stability of liquid film flow down an oscillating wall, J. Appl. Mech., Trans. ASME 58 (1991) 278.
[8] S.P. Lin, J.N. Chen, D.R. Woods, Suppression of instability of a liquid film flow, Phys. Fluids 8 (1996) 3247.
[9] J. Tihon, V. Penkavova, V. Sobolik, J. Drahos, Characteristics of waves on liquid films flowing down an oscillating inclined plane, in: Proc. 12th Congress Chem. Process Eng. CHISA '96, Prague, 1996.
[10] J. Drahos, J. Tihon, V. Sobolik, P. Hasal, I. Schreiber, J. Marek, Analysis of wave modes in liquid film falling down a vertical oscillating plate, Chem. Eng. Sci. 52 (1997) 1163.
[11] A. Oron, O. Gottlieb, Nonlinear dynamics of temporally excited falling liquid films, Phys. Fluids 14 (2002) 2622.
[12] T.R. Salamon, R.C. Armstrong, R.A. Brown, Traveling waves on vertical films: Numerical analysis using the finite element method, Phys. Fluids A 6 (1994) 2202.
[13] D.J. Benney, Long waves on liquid films, J. Math. Phys. 45 (1966) 150.
[14] B. Gjevik, Occurrence of finite-amplitude surface waves on falling liquid films, Phys. Fluids 13 (1970) 1918.
[15] O. Gottlieb, A. Oron, Stability and bifurcations of parametrically excited thin liquid films, Int. J. Bifurcation Chaos 14 (2004) 4417.
[16] S.W. Joo, S.H. Davis, Irregular waves on viscous falling films, Chem. Eng. Comm. 118 (1992) 111.
[17] B. Ramaswamy, S. Chippada, S.W. Joo, A full-scale numerical study of interfacial instabilities in thin-film flows, J. Fluid Mech. 325 (1996) 163.
[18] C. Ruyer-Quil, P. Manneville, Improved modeling of flows down inclined planes, Eur. Phys. J. B 15 (2000) 357.
[19] C. Ruyer-Quil, P. Manneville, Further accuracy and convergence results on the modeling of flows down inclined planes by weighted-residual approximations, Phys. Fluids 14 (2002) 170.
[20] V.Ya. Shkadov, Wave flow regimes of a thin layer of a viscous fluid subject to gravity, Izv. Akad. Nauk SSSR, Mekh. Zhidk. Gaza 2 (1967) 43. Also, translated in Fluid Dynam. 2 (1970) 29.
[21] H.C. Chang, Wave evolution on a falling film, Ann. Rev. Fluid Mech. 26 (1994) 103.
[22] H.C. Chang, E.A. Demekhin, D.I. Kopelevich, Nonlinear evolution of waves on a vertically falling film, J. Fluid Mech. 250 (1993) 433.
[23] T.B. Benjamin, Wave formation in laminar flow down an inclined plane, J. Fluid Mech. 2 (1957) 554.
[24] C.-S. Yih, Stability of liquid flow down an inclined plane, Phys. Fluids 6 (1963) 321.
[25] B. Scheid, C. Ruyer-Quil, U. Thiele, O.A. Kabov, J.C. Legros, P. Colinet, Validity domain of the Benney equation including Marangoni effect for closed and open flows, J. Fluid Mech. 527 (2005) 303.
[26] A. Oron, O. Gottlieb, E. Novbari, Numerical analysis of a weighted-residual integral boundary-layer model for nonlinear dynamics of falling liquid films, Eur. J. Mech. B/Fluids 28 (1) (2009) 1–36.
[27] E. Novbari, Nonlinear dynamics of thin liquid films on an inclined oscillating plane, M.Sc. Thesis, Technion – Israel Institute of Technology, Haifa, Israel, 2006.
[28] D.W. Jordan, P. Smith, Nonlinear Ordinary Differential Equations. An Introduction to Dynamical Systems, third ed., Oxford University Press, Oxford, 1999.
[29] A. Oron, Nonlinear dynamics of three-dimensional long-wave Marangoni instability in thin liquid films, Phys. Fluids 12 (2000) 1633.
[30] D. Gao, N.B. Morley, V. Dhir, Numerical simulation of wavy falling film flow using VOF method, J. Comp. Phys. 192 (2003) 624–642.
[31] T. Kunugi, C. Kino, DNS of falling film structure and heat transfer via MARS method, Comp. Struct. 83 (2005) 455–462.
[32] A. Miyara, Numerical simulation of wavy liquid film flowing down on a vertical wall and an inclined wall, Int. J. Therm. Sci. 39 (2000) 1015–1027.
[33] T. Nosoko, A. Miyara, The evolution and subsequent dynamics of waves on a vertically falling liquid film, Phys. Fluids 16 (2004) 1118–1126.
[34] C.D. Park, T. Nosoko, Three-dimensional wave dynamics on a falling film and associated mass transfer, AIChE J. 49 (2003) 2715–2727.
[35] J. Tihon, V. Tovchigrechko, V. Sobolik, O. Wein, Electrodiffusion detection of the near-wall flow reversal in liquid films at the regime of solitary waves, J. Appl. Electrochem. 33 (2003) 577–587.
[36] J. Tihon, K. Serifi, K. Argyriadi, V. Bontozoglou, Solitary waves on inclined films: their characteristics and the effects on wall shear stress, Exp. Fluids 41 (2006) 79–89.